Author Manuscript

Author Manuscript

Author Manuscript

Author Manuscript

HHS Public Access

Author manuscript

Cell Rep. Author manuscript; available in PMC 2023 May 15.

Published in final edited form as:

Cell Rep. 2022 November 22; 41(8): 111677. doi:10.1016/j.celrep.2022.111677.

Prenatal inflammation perturbs murine fetal hematopoietic development and causes persistent changes to postnatal immunity

Diego A. López[1,8], **April C. Apostol**[2,8], **Eric J. Lebish**[3], **Clint H. Valencia**[2], **Mari Carmen Romero-Mulero**[4], **Polina V. Pavlovich**[4], **Gloria E. Hernandez**[5], **E. Camilla Forsberg**[6], **Nina Cabezas-Wallscheid**[4], **Anna E. Beaudin**[7,9,*]

[1]Division of Microbiology and Immunology, Department of Pathology, University of Utah School of Medicine, Salt Lake City, UT, USA

[2]Quantitative and Systems Biology Graduate Program, University of California-Merced, Merced, CA, USA

[3]Department of Molecular and Cell Biology, University of California-Merced, Merced, CA, USA

[4]Max Planck Institute of Immunobiology and Epigenetics, 79108 Freiburg, Germany

[5]Molecular Biology Institute, University of California Los Angeles, Los Angeles, CA, USA

[6]Institute for the Biology of Stem Cells, University of California Santa Cruz, Santa Cruz, CA, USA

[7]Departments of Internal Medicine and Pathology, and Program in Molecular Medicine, University of Utah School of Medicine, Salt Lake City, UT, USA

[8]These authors contributed equally

[9]Lead contact

SUMMARY

Adult hematopoietic stem and progenitor cells (HSPCs) respond directly to inflammation and infection, causing both acute and persistent changes to quiescence, mobilization, and differentiation. Here we show that murine fetal HSPCs respond to prenatal inflammation *in utero* and that the fetal response shapes postnatal hematopoiesis and immune cell function. Heterogeneous fetal HSPCs show divergent responses to maternal immune activation (MIA), including changes in quiescence, expansion, and lineage-biased output. Single-cell transcriptomic analysis of fetal HSPCs in response to MIA reveals specific upregulation of inflammatory gene

This is an open access article under the CC BY-NC-ND license (http://creativecommons.org/licenses/by-nc-nd/4.0/).

*Correspondence: anna.beaudin@hsc.utah.edu.

AUTHOR CONTRIBUTIONS

Supervision, A.E.B.; study conceptualization, A.E.B. and E.C.F.; data collection and analysis, D.A.L., A.C.A., E.J.L., C.D.V., and G.E.H.; experimental design, data visualization, manuscript preparation, and manuscript revision, D.A.L. and A.C.A.; computational analysis, data visualization, and manuscript preparation, M.C.R.-M., P.P., and N.C.-W.; funding, A.E.B.

SUPPLEMENTAL INFORMATION

Supplemental information can be found online at https://doi.org/10.1016/j.celrep.2022.111677.

DECLARATION OF INTERESTS

The authors declare no competing interests.

Author Manuscript Author Manuscript Author Manuscript Author Manuscript

profiles in discrete, transient hematopoietic stem cell (HSC) populations that propagate expansion of lymphoid-biased progenitors. Beyond fetal development, MIA causes the inappropriate expansion and persistence of fetal lymphoid-biased progenitors postnatally, concomitant with increased cellularity and hyperresponsiveness of fetal-derived innate-like lymphocytes. Our investigation demonstrates how inflammation *in utero* can direct the output and function of fetal-derived immune cells by reshaping fetal HSC establishment.

Graphical Abstract

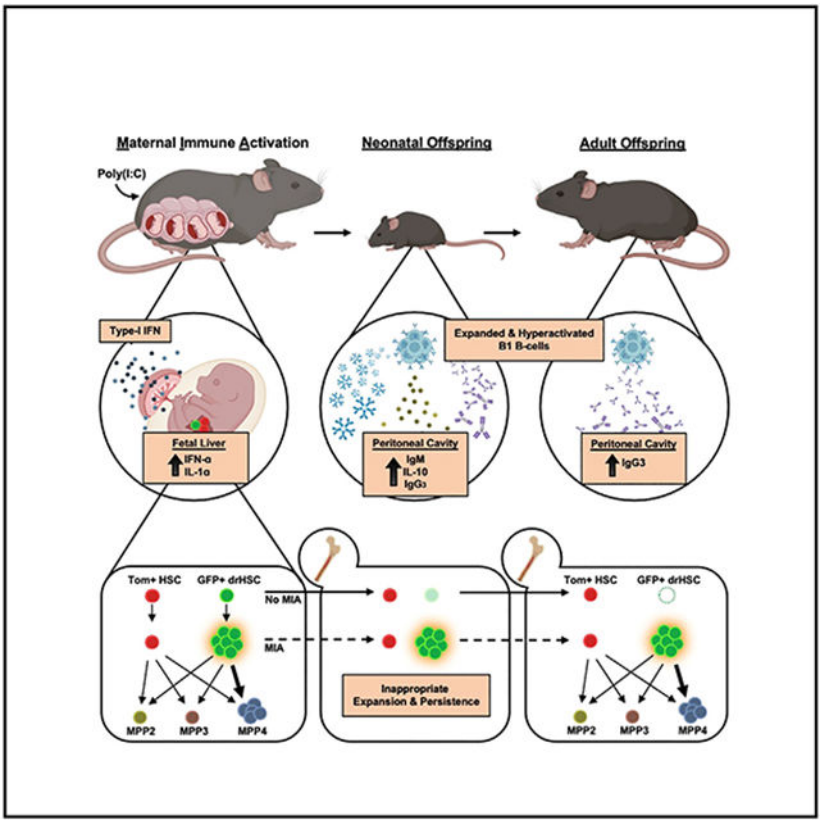

In brief

López et al. report that prenatal inflammation induces a lymphoid-biased hematopoietic response during fetal development, driven by the activation of a transient, lymphoid-biased hematopoietic stem cell. Postnatally, this results in sustained changes to the bone marrow progenitor compartment and accompanying expansion and hyperactivation of fetal-derived innate-like lymphocyte progeny.

INTRODUCTION

The adult immune system responds rapidly to infection by increasing the production of immune cells that control infectious microbes (Schultze et al., 2019; Takizawa et al., 2012). This response includes the release of inflammatory cytokines, mobilization and activation of immune cells, and increased production of immune cells from the bone marrow (BM) to

Author Manuscript Author Manuscript Author Manuscript Author Manuscript

eradicate microbes. The ability of the immune system to initiate a sustained and systemic response to infection is linked to the direct responsiveness of adult BM hematopoietic stem cells (HSCs) to inflammatory signals. Adult HSCs respond to both cytokines and Toll-like receptor (TLR) ligands *in situ* (Baldridge et al., 2010; Esplin et al., 2011; Essers et al., 2009; Furusawa et al., 2016; Nagai et al., 2006; Pietras et al., 2016; Schuettpelz and Link, 2013; Takizawa et al., 2017; Yamashita and Passegué, 2019), driving both acute and long-term changes to HSC function that shape the immune response.

In response to inflammation or infection, adult HSCs exit quiescence (Essers et al., 2009) and show accentuated myeloid bias (Matatall et al., 2014; Pietras et al., 2016) and increased myeloid output, leading to the production of sufficient quantities of myeloid cells required to combat infection. Accumulating evidence suggests that, in response to both normal and aging-related inflammation, myeloid-biased output is propagated both by the disparate activation of myeloid-biased HSCs (Beerman et al., 2010; Haas et al., 2015; Matatall et al., 2014), and the downstream expansion of myeloid-biased multipotent progenitors at the expense of lymphoid progenitors (Pietras et al., 2016). Furthermore, persistent responsiveness of hematopoietic stem and progenitor cells (HSPCs) to inflammatory signals, programmed by chromatin modifications and metabolic alterations, has been suggested to underlie long-term functional changes to infection described in short-lived myeloid cells (Chavakis et al., 2019; Kaufmann et al., 2018; Mitroulis et al., 2018). These data suggest that inflammation can program long-term immune output from hematopoietic progenitors that has consequences for immune function.

Prenatal inflammation and infection shape the postnatal immune response, including susceptibility to infection, hypersensitivity disorders, and response to vaccination (Apostol et al., 2020). Several studies have demonstrated that prenatal inflammation can program alterations to mature immune cell output (Hsiao et al., 2012; Mandal et al., 2010, 2011, 2013), but the drivers of persistent changes to offspring immunity are poorly understood. In the developing embryo, "sterile" inflammatory signaling is required for HSC emergence in early development (Espin-Palazon et al., 2018). However, beyond emergence, there is little information regarding whether developing HSCs respond *in utero* to maternal inflammation, how they respond, and the consequences for postnatal hematopoietic and immune development. We hypothesize that the fetal HSC response to prenatal inflammation drives lasting changes to hematopoietic output in offspring that shapes the postnatal immune response.

Here, we use a maternal immune activation (MIA) model to decipher the effects of *in utero* inflammation on fetal HSPCs, and examine the long-term impact to postnatal hematopoietic and immune system establishment. In direct contrast to myeloid bias invoked by inflammation in adult hematopoiesis, our *in vivo* analysis and single-cell transcriptional profiling reveal that prenatal inflammation evokes lymphoid bias by specifically activating transient, lymphoid-biased fetal HSCs. The activation and inappropriate persistence of otherwise transient lymphoid-biased fetal HSCs leads to functional changes to postnatal hematopoiesis and immune output, including increased production and activity of fetal-derived innate-like lymphocytes. By demonstrating that fetal HSPC heterogeneity underlies

Author Manuscript Author Manuscript Author Manuscript Author Manuscript

a differential response of prenatal hematopoiesis to inflammation, our findings have important implications for defining developmental origins of immune dysfunction.

RESULTS

Prenatal inflammation induced by MIA causes expansion of a developmentally restricted HSC

To investigate how fetal HSPCs respond to maternal inflammation, we used a mouse model of MIA (Meyer et al., 2009) that mimics a mild viral infection in pregnant mice with a single intraperitoneal (i.p.) injection of the TLR3 agonist polyinosinic:polycytidylic acid (pIC). We performed these experiments using the FlkSwitch mouse model (Boyer et al., 2011), which identifies a developmentally restricted, lymphoid-biased HSC (drHSC) with specific potential to produce fetal-restricted immune cells, including B1-B cells (Beaudin et al., 2016). In the FlkSwitch model, Flk2-driven expression of Cre results in a permanent genetic switch from Tomato (Tom) to GFP expression (Boyer et al., 2011). Both Tom+ and GFP+ HSCs are present during perinatal development (Figure 1A), but only Tom+ HSCs persist and contribute functionally to the adult HSC compartment (Boyer et al., 2011, 2012). We denote Tom+ HSCs in the fetal liver (FL) as conventional HSCs, and GFP+ HSCs in the FL as developmentally restricted HSCs, or GFP+ drHSCs (Beaudin et al., 2016).

To induce MIA, we injected pregnant C57BL/6J (wild-type [WT]) females crossed to FlkSwitch males with 20 mg/kg pIC or saline control at embryonic day (E)14.5, when HSPCs in the FL undergo massive expansion. We examined HSPCs in offspring 1-3 days later, postnatally, and into adulthood (Figure 1A). The dose of pIC used produced no obvious signs of illness in the mother. Crown-rump length (CRL) of E15.5 fetuses was lower in MIA litters compared with saline-treated litters (Figure S1A), and onset of birth was delayed by 1 day in 35% of litters born (Figure S1B). By postnatal day (P)14, there was a slight reduction in surviving pups from MIA (Figure S1C) although those pups were on average larger than controls (Figure S1D), most likely due to longer gestation time (Figure S1B).

Clear changes to the fetal hematopoiesis were observed 1 day after MIA induction. HSPCs (CD45+, Lineage−, cKit+, Sca1+) showed a marked increase in frequency 1 day after injection (Figures 1B and 1C) that was normalized by E17.5 (Figure 1D). Despite increased HSPC frequency, HSPC cellularity at E15.5 was not significantly increased (Figure S1E), reflecting an overall decrease in CD45+ cells in the FL (Figure S1F). Importantly, compared with adult BM HSPCs (Figures S2A and S2B), MIA did not induce Sca1 upregulation in the FL (Figure S2C), including in CD45+ cells (Figure S2D) or long-term (LT) HSCs (Figures S2E and S2F), suggesting that increased fetal HSPC frequency was not caused by interferon (IFN)-induced Sca1 upregulation. Indeed, although fluorescein-labeled pIC crossed the placenta and could be detected within FL cells (Figure S2G), FL HSPCs did not express detectable TLR3, suggesting that they did not respond directly to pIC (Figure S2H). Frequency of GFP-labeled cells was significantly increased across all HSPCs (Figure 1E), consistent with progenitor expansion. Cellularity of LT-HSCs (CD45+ Lin−, cKit+, Sca1+, CD150+, CD48−; Figure 1F), including Tom+ HSCs (CD45+, Lin−, cKit+, Sca1+, CD150+, Tom+; Figure 1G) was unchanged from E15.5-E17.5 in response to MIA. In contrast, we

Author Manuscript Author Manuscript Author Manuscript Author Manuscript

observed a significant spike in the number of GFP+ drHSCs (CD45+, Lin−, cKit+, Sca1+, CD150+, GFP+) 1 day following MIA, after which cellularity returned to control levels by E16.5 (Figure 1H).

To examine the mechanism underlying the specific expansion of the GFP+ drHSCs in response to MIA, we assessed proliferation at E15.5. MIA drove increased proliferation of both Tom+ HSCs and GFP+ drHSCs (Figures 1I and 1J), but MIA drove virtually all GFP+ drHSCs out of G0 (Figures 1I and 1J). Importantly, only increased proliferation of GFP+ drHSCs corresponded to a significant increase in cellularity 1 day later (Figure 1H).

Activation of a developmentally restricted HSC drives downstream expansion of lymphoid-biased multipotent progenitors

As MIA induced a rapid response by HSCs that coincided with an increase in overall GFP expression across all HSPCs (Figure 1H), we next examined how downstream progenitors responded to MIA, including short-term (ST)-HSCs and multipotent progenitor (MPP) subsets (Pietras et al., 2015) (Figure 2A). Cellularity of myeloid-biased ST-HSCs, MPP2, and MPP3 cells were unaffected by MIA (Figures 2B-2D), an observation that deviates from previously reported dynamics in the adult hematopoietic response to inflammation (Pietras, 2017). Committed myeloid progenitors were also not expanded in response to MIA (Figures S2G and S2I). In contrast, lymphoid-biased Flk2+ MPP4s were significantly expanded 2 days post MIA compared with controls (Figure 2E). Expansion of Flk2+ MPP4s did not immediately translate into expansion of downstream committed lymphoid progenitors or mature lymphoid cells (Figures S1H, S1J, and S1K), as expected based on differentiation dynamics of lymphoid lineages (Busch et al., 2015). CD150− MPPs showed increased proliferation at E15.5 and E16.5 (Figures 2F and 2G), likely driving the significant increase in cellularity of MPP4s at E16.5. Expansion of both lymphoid-biased GFP+ drHSCs and Flk2+ MPP4s in response to MIA suggested that prenatal inflammation specifically evoked a lymphoid-biased response in fetal progenitors.

We previously demonstrated that the GFP+ drHSC is lymphoid-biased and lymphoid-lineage primed (Beaudin et al., 2016). To directly test whether expanded GFP+ drHSCs contributed to the increase in MPP4s, we isolated Tom+ HSCs and GFP+ drHSCs from FL 2 h post saline or MIA induction, cultured them *ex vivo* over 24 h, and measured HSPC output (Figures 2H and S2I). After 24 h, both Tom+ HSCs and GFP+ drHSCs produced all HSPC subsets, but GFP+ drHSCs generated significantly more MPP4s compared with Tom+ HSCs under saline conditions (Figure 2I). Importantly, although MPP output from Tom+ HSCs was unchanged after MIA treatment, MPP4 output from GFP+ drHSCs was further exaggerated by MIA, at the expense of other MPP subsets (Figure 2I).

Prenatal inflammation induced by MIA affects self-renewal and hematopoietic output of developing HSCs

To investigate how MIA affected function and output of Tom+ HSCs and GFP+ drHSCs, we performed competitive transplantation assays with isolated Tom+ HSCs or GFP+ drHSCs from E15.5 FL 1 day post MIA or saline treatment (Figure 3A). Under control conditions, fewer recipients of GFP+ drHSCs were reconstituted compared with recipients of Tom+

Author Manuscript Author Manuscript Author Manuscript Author Manuscript

HSCs (Figure 3B), and GFP+ drHSC recipients demonstrated lymphoid-biased contribution to peripheral blood (PB) output (Figure S3A), as previously reported (Beaudin et al., 2016). In primary transplantation, MIA did not affect frequency of recipients exhibiting long-term multilineage reconstitution (LTMR) for either Tom+ HSCs or GFP+ drHSCs (Figure 3B). MIA induced significantly increased granulocyte-monocyte (GM) output in PB (Figure 3C) of primary Tom+ HSC recipients, although there were no differences in BM chimerism of HSPCs (Figures S2B and S2C), myeloid progenitors, lymphoid progenitors, or mature cells after 18 weeks (Figures S3D and S3E). MIA did not affect PB (Figure 3C) or BM progenitor output (Figures S3B-S3E) in primary recipients of GFP+ drHSCs. In sharp contrast, LTMR was significantly impaired in secondary recipients of Tom+ HSCs (Figure 3D), whereas the effect of MIA in secondary recipients of GFP+ drHSCs was less severe. Tom+ HSC exhaustion was evident in both PB output (Figure 3E) and BM progenitor chimerism in MIA-treated Tom+ HSC secondary recipients (Figures S3G-S3J). In contrast, secondary recipients of GFP+ drHSCs did not exhibit any functional differences in response to MIA: both PB and BM chimerism were unaffected by MIA, and lymphoid-biased output was sustained (Figure 3E; Figure S3F). Together, serial transplantation assays revealed a disparate response of two fetal HSC populations, with an initial myeloid bias followed by subsequent loss of self-renewal potential in Tom+ HSCs, but not GFP+ drHSCs, following MIA.

Single-cell sequencing reveals the response of distinct fetal HSPCs to MIA

To understand how MIA remodels hematopoietic development at the molecular level, we sorted E15.5 FL HSPCs from MIA or saline-treated dams and analyzed the transcriptional profiles of 23,505 cells using single-cell RNA sequencing (scRNA-seq). Unsupervised clustering analysis identified 14 distinct clusters (C0–C13) (Figures 4A and S4A). Clusters segregated based on differential gene expression profiles and cell-cycle states (Figure S4B). We specifically focused our analysis on how distinct clusters responded to MIA in order to gain insight into the response of a heterogeneous fetal HSPC compartment to prenatal inflammation. MIA altered the distribution of cells across clusters (Figures 4B and 4C). A differential response to MIA was observed among most clusters: C1, C3, C5, C6, C9, and C10 were robustly expanded in response to MIA, whereas C2, C4, C7, and C8 were significantly reduced in response to MIA (Figure 4D).

We utilized our published dataset (Beaudin et al., 2016) to determine overlap of the phenotypic FL GFP+ drHSCs and Tom+ HSCs with our identified clusters. This resulted in the emergence of two divergent regions encompassing multiple clusters enriched for Tom+ HSC (Figures 4E and 4G) or GFP+ drHSC signature (Figures 4F and 4H). Several clusters that expanded in response to MIA significantly overlapped with the GFP+ drHSC signature (C1, C3, C5, C9, and C10), whereas clusters decreasing in response to MIA overlapped with the Tom+ HSC signature (C2, C4, C7, and C8). TdTomato and eGFP transcript expression was also enriched in clusters overlapping with Tom+ HSC and GFP+ drHSC signatures, respectively (Figure S4C), although overlap was not precise due to broad GFP expression across MPPs within the FlkSwitch model (Boyer et al., 2011).

Author Manuscript Author Manuscript Author Manuscript Author Manuscript

To annotate clusters responding to MIA, we determined HSC and MPP identity based on adult transcriptional profiles (Cabezas-Wallscheid et al., 2014). Clusters segregated into either HSC- (Figures 4I and 4K) or MPP-like populations (Figures 4J and 4L), and two clusters, C2 and C9, were the most enriched for HSC identity with no significant enrichment for MPP genes. Gene set enrichment analysis (GSEA) of HSC-like C2 revealed best concordance with Tom+ HSC identity (Figure 4M) and was defined by a quiescent cell-cycle state (Figure S4B) and by expression of canonical HSC genes, including *Mecom* (Figure S4A), *Hlf* (Figure S4A), *Mllt3* (Figure S4D), and Meis1 (Figure S4E) (Gazit et al., 2013). The remaining Tom+ HSC clusters (C0, C4, C7, C8, and C13; Figure 4G) overlapped with both HSC and MPP signatures (Figures 4I-4L) and showed significant enrichment of megakaryocyte-associated genes (Figure S4F) and no enrichment for lymphoid- (Figure 4O) or myeloid-associated genes (Figure S4G). The identification of HSC-like C2 within the clusters most enriched for Tom+ HSC identity is consistent with HSC activity within the Tom+ HSC fraction.

Clusters enriched for the GFP+ drHSC signature (C1, C3, C5, C9 10, C11, and C12; Figure 4H) exhibited varying degrees of stemness (Figures 4I-4L) and lymphoid (Figure 4O) and myeloid priming (Figure S4G). C9 was specifically enriched for both GFP+ drHSC signature (Figures 4F and 4H) and adult HSC signature (Figure 4K). Additionally, C9 was the only cluster to be significantly enriched for lymphoid-, myeloid-, and megakaryocyte-associated genes (Figures 4O, S4F, and S4G). Although C9 did not express the same set of canonical HSC genes expressed by C2, C9 expressed other canonical and non-canonical HSC markers, including HLA genes (Figure S4A), *Spi1* (Staber et al., 2013) (Figure S4H), *Pbx1* (Ficara et al., 2008) (Figure S4I), *Cd74* (Luckey et al., 2006) (Figures S4A and S4J), and *Tet2* (Moran-Crusio et al., 2011) (Figure S4K). C9 was heterogeneous for cell-cycle markers (Figure S4B), with a subset of cells appearing highly quiescent. C5, C9, C10, C11, and C12 were all highly enriched for lymphoid gene signature (Figure 4O), while C1, C5, C9, C11, and C12 were all enriched for myeloid gene signature (Figure S4G). Notably, C10 expressed genes important for early B cell and innate-like B cell development and identity, including *Vpreb1/3, Ccr9, Ebf1, Ighm, Chchd10*, and *Mzb1* (Figures 4P-4S), and was particularly enriched for the GFP+ drHSC signature (Figure 4H). Furthermore, MIA accentuated lymphoid-lineage priming in C10, as demonstrated by significant upregulation of the same lymphoid-associated genes (Figures 4T-4W). Importantly, overlap of multiple stem cell-, lymphoid-, and myeloid-associated clusters with the phenotypically defined GFP+ drHSC reflects both multipotency and lymphoid bias of the GFP+ drHSC *in vivo*.

Fetal HSPCs respond distinctly to inflammatory cytokines induced by MIA

In utero, the fetus may be passively exposed to maternal cytokines through the placental barrier or, alternatively, fetal cells may initiate a discrete fetal immune response to maternal inflammation (Apostol et al., 2020). To interrogate potential signaling mechanisms driving the specific response of lymphoid-biased FL HSPCs, we compared inflammatory cytokine profiles in maternal serum, amniotic fluid (AF), and FL supernatant 1 day post MIA, at E15.5. IFN-α and interleukin (IL)-23 were significantly increased in maternal serum (Figures 5A and S2J). In AF, levels of IFN-α, IFN-β, IL-27, and GM colony-stimulating factor (GM-CSF) were increased in response to MIA (Figures 5B and 5C). In contrast,

Author Manuscript Author Manuscript Author Manuscript Author Manuscript

the FL only exhibited upregulation of two cytokines: IL-1α and IFN-α (Figures 5D and 5E). The increase in type I IFNs in the maternal serum, AF, and FL suggest that type I IFN-mediated inflammation is evoked from either the maternal response (Figures 5 and S2J) or non-HSPC populations in FL, as IFN-α, IFN-β, and IL-1α cytokine was not produced directly from HSPCs (data not shown). HSPCs also did not express TLR3 (Figure S2H), suggesting they did not respond directly to pIC.

To profile possible interactions between fetal HSPCs and cytokines observed in the fetal microenvironment, we scored enrichment of immune-related cytokine signaling gene signatures in our scRNA-seq data. Only C9, a stem cell-like cluster that overlapped significantly with the GFP+ drHSC expression signature, was significantly enriched for expression of genes associated with immune cytokine signaling (Figure 5F). Further examination of IL-1α and IFN-α signaling (cytokines upregulated in the FL following MIA; Figures 5D and 5E) revealed significant enrichment for IFN signaling pathways within C9 (Figure 5G). In particular, IFN-stimulated genes (ISGs) *Stat1*, *Isg15*, and *Ifi27l2a* were highly expressed within C9 and increased expression following MIA (Figure 5H). In contrast, overall IL-1 signaling expression was unchanged or decreased across clusters following MIA (Figure S2K), suggesting that IFN-α signaling is a major driver of the fetal HSPC inflammatory response.

To further elucidate the response of fetal HSPCs to type I IFNs, we crossed mice expressing Cre recombinase under control of the IFN-inducible Mx1 promoter ($Mx1^{Cre}$) to an Ai9 reporter mouse ($R26^{LSL\text{-}tdTomato}$) and ascertained labeling of fetal HSPCs 1, 24, and 72 h following pIC or saline control (Figure 5I). Mx1-Cre labeling at 1 h in response to MIA was evident across all HSPCs via Tomato (Tom+) expression (Figure 5J). By 24 h post MIA, labeling was significantly enriched in ST-HSCs. After 72 h, ST-HSCs exhibited the highest degree of labeling, and LT-HSCs also showed significantly increased labeling. MPP4s similarly exhibited a significant labeling 72 h post MIA, whereas labeling of MPP2 and MPP3 subsets did not significantly increase over time (Figure 5J). Minimal labeling was observed in myeloid progenitors (cKit+ Sca1− CD45+ Lin−; Figure S2L) and B1 B cells (Figure S2M) 24 h post MIA. As activation of the Mx1 promotor is stringent and transient, even under continued exposure to type-1 IFNs in culture (Staeheli et al., 1986), the increased labeling in ST-HSCs over time reflects expansion of labeled cells after pIC induction, rather than *de novo* Mx1-Cre labeling. Because FL GFP+ drHSCs are enriched in the $CD150^{mid}$ LSK fraction in FlkSwitch mice, the increased label of ST-HSCs in $Mx1^{Cre}$Ai9 mice likely reflects combinatory labeling of both GFP+ drHSCs and ST-HSCs, the former demonstrating greater proliferation and cellularity 24 h post MIA (Figures 5H-5J). Although ST-HSCs exhibited the greatest increase in label 24–72 h post MIA, ST-HSC cellularity did not increase *in vivo* (Figure 2B), whereas GFP+ drHSCs were significantly expanded 1 day after MIA induction, followed by significantly increased MPP4 cellularity 2 days post MIA. Together, these data suggest that the response to MIA is driven by an immediate HSC response to type-1 IFNs.

Author Manuscript Author Manuscript Author Manuscript Author Manuscript

Developmental effects of prenatal inflammation on hematopoiesis persist postnatally

As MIA perturbed fetal hematopoiesis, we next sought to determine if MIA affected hematopoiesis in the postnatal period. At P14, we observed sustained expansion of frequency and number of HSPCs in MIA-treated offspring (Figures 6B and 6C). LT-HSCs were unchanged in response to MIA (Figure 6D), but demarcation of LT-HSCs into Tom+ HSCs and GFP+ drHSCs revealed specific expansion of GFP+ drHSCs (Figure 6F) in the absence of changes to Tom+ HSCs (Figure 6E). Expansion of HSPCs could be attributed almost entirely to a 2-fold expansion of Flk2+ MPP4s (Figure 6G), whereas other MPP subsets (Figure 6H) and myeloid progenitors (Figure S5G) were unchanged. We observed this precise pattern in response to MIA during the fetal period, suggesting a lasting and specific effect of MIA on HSPCs. Importantly, deletion of TLR3 in the pregnant dam, which effectively isolated the direct response of the fetus to pIC, eliminated the effect of MIA on postnatal hematopoiesis (Figure S5H). These data confirm that expansion of lymphoid-biased GFP+ drHSCs and Flk2+MPP4s was driven by a maternal type I IFN response and not by the direct response of fetal HSPCs to pIC.

We next examined whether prenatal inflammation could drive lasting changes to adult hematopoiesis (Figures 6I-6P and S5A-S5F). MIA caused a sustained expansion of HSPC frequency into adulthood (Figures 6I-6K), and a specific increase in frequency of adult lymphoid-biased MPP4s (Figure 6O), whereas cellularity and frequency of all other MPP subsets and myeloid progenitors were not significantly affected (Figures S5E, S5F, and S5I). Frequency (Figures 6L and 6M) and cellularity (Figures S5B and S5C) of LT-HSCs and Tom+ HSCs were not affected by MIA. Although we have previously demonstrated both phenotypically (Boyer et al., 2011) and functionally (Boyer et al., 2012) that GFP+ drHSCs are virtually absent within adult BM, GFP+ cells were present within the phenotypic LT-HSC compartment in saline-treated adults (Figures 6N and 6P). Nonetheless, we observed sustained expansion of GFP+ drHSCs into the adult BM by both frequency (Figure 6N) and cellularity (Figure 6P) in MIA-treated adult offspring compared with controls. These data suggest that prenatal inflammation during fetal development imparts specific and lifelong changes to HSPC cellularity that can be traced well into adulthood.

Persistent changes to hematopoiesis induced by prenatal inflammation affect innate-like immune cell function

GFP+ drHSCs specifically generate fetal-derived innate-like lymphocytes during development, including B1 B cells and marginal zone (MZ) B cells (Beaudin et al., 2016). As MIA caused persistent changes to the developing HSC compartment, we hypothesized that the inappropriate expansion of the GFP+ drHSC would subsequently affect the establishment of their innate-like immune cell progeny. We enumerated innate-like B cells in the peritoneal cavity (PerC) and MZ of the spleen in offspring of MIA- and saline-treated litters at P14 (Figures 7A-7C). Although conventional B2 cells were unchanged in response to MIA, both CD5+ B1-a cells and CD5− B1-b cells were significantly expanded in P14 offspring following MIA (Figure 7A) and thereafter cellularity normalized by adulthood (Figure S5J). Similarly, MIA increased cellularity of splenic MZ B cells (Figure 7B), whereas conventional follicular B2 cells were unchanged (Figure 7C). Notably, fetal B cells did not expand during the fetal period in response to MIA (Figures S1H and S1K) and

Author Manuscript Author Manuscript Author Manuscript Author Manuscript

were not IFN responsive (Figure S2K), suggesting that postnatal expansion was due directly to an expanded GFP+ drHSC precursor. These data suggest that sustained changes to the HSC compartment led to measurable differences in fetal-derived innate-like immune cells postnatally.

B1 B cells function as a first line of immunity in neonates by producing “natural” antibodies (Baumgarth, 2011; Montecino-Rodriguez and Dorshkind, 2006). To define whether observed changes in innate-like lymphocyte cellularity also translated into changes in postnatal cellular function, we profiled natural antibody production in offspring following MIA (Figures 7D-7F). Coincident with expanded B1-B cell cellularity, MIA-treated offspring produced significantly more natural antibody, including immunoglobulin (Ig) M (Figure 7D) and IgG3 (Figure 7F) in the PerC, whereas total IgG was unchanged (Figure 7E). B1-B cells from MIA-treated offspring also produced more IL-10 upon stimulation (Figure 7G), suggesting a greater responsiveness to secondary immune challenge. Importantly, these results were normalized for cell number, suggesting that B1-B cells from MIA-treated offspring produced more natural antibody on a per-cell basis. Surprisingly, while total PerC IgM production normalized in adult offspring (Figure 7H), we observed a persistent and significant increase in total IgG3 production (Figure 7I) in adult MIA-treated offspring. These data suggest that the early hematopoietic response to *in utero* inflammation not only reshapes HSC function and establishment but also alters output and function of developmentally regulated immune cells.

DISCUSSION

Adult HSCs respond directly to inflammation, resulting in both acute and sustained changes to HSC function that drive the systemic immune response to infection (Pietras, 2017). Although, in the adult BM, HSCs are directly exposed to pathogens, cytokines, and inflammatory mediators through circulation, exposure of the fetus to prenatal inflammation is limited by the maternal-fetal barrier (Ander et al., 2019). Little is known regarding how *in utero* inflammation might be interpreted by the developing fetal immune system, and, to our knowledge, there has been no direct investigation of how *in utero* inflammation directly influences fetal hematopoiesis. Here we demonstrate that developing fetal HSCs respond directly to *in utero* inflammation. We used a mouse model of MIA, in which injection of pIC at midgestation mimics an immune response to viral infection during pregnancy (Meyer et al., 2009). Although MIA does not model the complex nature of an actual congenital infection, MIA allowed us to distill the effect of *in utero* inflammation in the absence of overt fetal infection. We performed these experiments using our FlkSwitch model (Beaudin et al., 2016; Boyer et al., 2011), in which we have previously described two distinct fetal progenitors: a Tom+ HSC that persists into adult BM, and a lymphoid-biased, GFP+ drHSC that is transient and exists only in the perinatal period. This platform allowed us to test the response of a heterogeneous fetal hematopoietic compartment to inflammation *in utero*. Our investigation revealed that prenatal inflammation specifically activates an immediate and sustained response in otherwise transient fetal progenitors, thereby affecting the output and function of fetal-derived immune cells.

Author Manuscript Author Manuscript Author Manuscript Author Manuscript

Adult hematopoietic progenitors exhibit myeloid bias and increased myeloid output in response to inflammation (Haas et al., 2015; Matatall et al., 2014; Pietras et al., 2016) that is propagated both by the specific activation of myeloid-biased HSCs (Beerman et al., 2010; Gekas and Graf, 2013; Haas et al., 2015; Mann et al., 2018), as well as the downstream expansion of myeloid-biased progenitors (Pietras et al., 2016). In sharp contrast, our analysis revealed that inflammation during the fetal period invoked a lymphoid-biased response by activating lymphoid-biased fetal GFP+ drHSCs and driving the downstream expansion of lymphoid-biased Flk2+ MPP4s. GFP+ drHSCs preferentially generate MPP4s, a bias that was exaggerated upon MIA induction. Expansion of GFP+ drHSCs 1 day post MIA is therefore responsible for subsequent expansion of Flk2+ MPP4s 1 day later, and sustained expansion of both populations was also observed postnatally. Our analysis of the initial response of HSPCs to IFNs using the Mx1-Cre model similarly confirmed that HSCs drive the initial response to MIA. Together, our data indicate that inflammation induced by MIA during the fetal period invokes a lymphoid-biased response *in situ* by activating lymphoid-biased HSCs that subsequently drive the downstream expansion of lymphoid-biased progenitors. It is possible that more complex infections with diverse cytokine responses may invoke a distinct response from a highly heterogeneous fetal HSPC compartment.

In contrast to the lymphoid-biased hematopoietic response observed *in situ*, adoptive transfer experiments revealed that Tom+ HSCs exhibited higher GM chimerism upon transplantation, suggesting the possibility that MIA also activated Tom+ HSCs and induced myeloid bias. However, neither expansion of Tom+ HSCs nor myeloid bias was observed *in situ*. Similarly, although enhanced lymphoid differentiation was observed *ex vivo* and *in situ* in response to MIA, MIA did not exaggerate lymphoid bias in GFP+ drHSCs upon transplantation. This discrepancy in the *in situ* response compared with the output of HSCs upon transplantation could be due to exposure to different microenvironmental cues in an irradiated, adult environment (Guo et al., 2017). Alternatively, these data suggest that prenatal inflammation does not change the cell-intrinsic bias of fetal HSCs, but instead activates and expands specific subsets within the FL microenvironment. Interestingly, serial transplantation resulted in rapid exhaustion of Tom+ HSCs, but not GFP+ drHSCs, although GFP+ drHSCs exhibited lower chimerism overall upon serial transplantation, as previously described (Beaudin et al., 2016). This is consistent with MIA inducing abnormal persistence of the GFP+ drHSC, potentially at the expense of persistence of some fraction of the Tom+ HSCs. Fundamental differences in the composition of adult and fetal hematopoietic compartments (Beaudin et al., 2016; Benz et al., 2012; Böiers et al., 2013; Crisan et al., 2016; Li et al., 2020) may underlie divergent hematopoietic trajectories between fetal and adult hematopoiesis in response to inflammation. Specifically, activation of a transient, lymphoid-biased fetal HSC may reflect the increased sensitivity of transient fetal progenitors to prenatal inflammation as a mechanism to prime the developing immune system. Coupled with the concept of layered immunity (Herzenberg, 1989), specialized subsets of immune cells, such as B1-B cells, may also be more receptive to insult during the prenatal period. Susceptibility of adult HSC precursors, and the long-term effects of prenatal inflammation on their self-renewal capability, output, and response to infection, requires additional investigation.

Author Manuscript Author Manuscript Author Manuscript Author Manuscript

scRNA-seq of over 23,000 fetal HSPCs confirmed the expansion of both HSC-like progenitors and lymphoid-primed progenitors in response to MIA. Two clusters, C2 and C9, resembled HSCs in both transcriptional profile and proliferative state, but only C9 overlapped transcriptionally with the GFP+ drHSC and was expanded in response to MIA. C9 was also the only cluster to exhibit a strong cytokine-responsive transcriptional profile, and increased inflammatory gene expression in response to MIA, suggesting that other cytokines would similarly evoke a lymphoid-biased response from C9. IFN-α was upregulated in the FL, and C9 also exhibited a robust transcriptional response to IFN. Surprisingly, upregulation of type I IFNs did not increase non-specific Sca1 expression in the fetus, as observed in adult hematopoiesis (King and Goodell, 2011). In contrast, C2, which overlaps transcriptionally with the Tom+ HSC, exhibited a more adult-like HSC profile, including expression of canonical HSC genes *Mllt3* and *Meis1*. Furthermore, C2 contracted in response to MIA, and expressed little to no inflammatory gene signature. Our transcriptional analysis mirrors our *in vivo* data, whereby we identified an HSC-like cluster, overlapping with the GFP+ drHSC, that both expands and exhibits a robust transcriptional response to cytokines that are upregulated within the fetal microenvironment in response to MIA.

Our scRNA-seq also identified a highly lymphoid-biased cluster, C10, that overlapped transcriptionally with the GFP+ drHSC signature. Not only did MIA significantly expand C10 but we also upregulated expression of lymphoid-associated genes such as *Ighm, Chchd10, Mzb1*, and *Vpreb 1/3* in response to MIA. Notably, many of these genes are associated with B cell and innate-like B cell lineage commitment, possibly skewing toward postnatal production of hyperactivated innate-like B cells. Whether increased expression of lymphoid-associated genes in fetal progenitors ultimately contributes to a hyperactivated phenotype postnatally remains to be determined. Nonetheless, this profile parallels our *in vivo* observation of specific expansion of lymphoid-biased progenitors in response to MIA, and provides additional evidence that prenatal inflammation drives lymphoid bias during the fetal and postnatal period.

The MIA model is widely used to examine how prenatal inflammation affects brain development during a critical window (Meyer et al., 2009). A critical window refers to a developmental window during which extrinsic or intrinsic inputs can shape the phenotype of the adult organism. Here, we use the same approach to establish a framework for a critical window for hematopoietic and immune development wherein extrinsic input, in the form of *in utero* inflammation, shapes the establishment and output of the hematopoietic and immune systems. Although it was previously reported that, under homeostatic conditions, the GFP+ drHSC fails to persist into adulthood (Beaudin et al., 2016; Beaudin and Forsberg, 2016), here we observed the persistence of some phenotypic GFP+ drHSCs into adulthood. We believe this is due to increased basal inflammation within our mouse colony, which fits with our observation that persistence of GFP+ drHSCs is induced by prenatal inflammation, as well as basal labeling by Mx1-Cre in the absence of MIA. Nonetheless, heightened inflammation induced by MIA drove increased proliferation, expansion, and enhanced persistence of GFP+ drHSCs postnatally and into adulthood. Concomitant with postnatal expansion of GFP+ drHSCs, we observed the specific expansion and hyperactivation of fetal-derived innate-like lymphocytes. Fetal B cells did not expand in direct response to

Author Manuscript Author Manuscript Author Manuscript Author Manuscript

prenatal inflammation induced by MIA, nor were they directly response to IFNs. Although we cannot directly track progeny of the GFP+ drHSC *in situ*, due to limitations of the FlkSwitch model (Boyer et al., 2012), the coincidence of expanded and activated GFP+ drHSCs, and their innate-like lymphocyte progeny in response to prenatal inflammation strongly suggests a causal relationship. These data suggest that prenatal inflammation during fetal development can shape postnatal hematopoietic and immune output. We did not directly test the effect of an expanded and hyperactivated B1 B cell compartment on offspring immunity. However, hyperactivated B1 B cells and increased natural antibody could be expected to protect neonates from severe infections such as sepsis (Baumgarth, 2021; Smith and Baumgarth, 2019), although elevated IL-10 levels might also increase susceptibility (Romagnoli et al., 2001; Ye et al., 2017). Together, our results illuminate how *in utero* inflammation can influence immune trajectories by reshaping hematopoiesis during development. Our discovery has significant implications for understanding the ontogeny of many immune-related disorders with poorly understood etiology, including diseases of tolerance and autoimmunity. Future studies should directly address how lasting changes to immune output and function modulate susceptibility to infection and disease.

Limitations of the study

While MIA is a widely used and accepted model to study postnatal outcomes associated with prenatal inflammation, there are limitations associated with translating our results to actual congenital infections.

In this study, we determined the persistent effects of prenatal inflammation on postnatal immune function by defining expansion of specific fetal-derived immune populations and examining cellular function in those specific populations. Future studies should more directly examine immune outcomes (i.e., response to infection) associated with these changes in response to prenatal inflammation.

STAR★METHODS

RESOURCE AVAILABILITY

Lead contact—Further information and requests for resources and reagents should be directed to and will be fulfilled by the Lead contact, Anna E. Beaudin (anna.beaudin@hsc.utah.edu).

Materials availability—This study did not generate new unique reagents.

Data and code availability

- The accession number for GEO where the RNA-seq datasets generated in this study are available is GSE161927.
- This paper does not report original code.
- Any additional information required to reanalyze the data reported in this paper is available from the lead contact upon request.

Author Manuscript Author Manuscript Author Manuscript Author Manuscript

EXPERIMENTAL MODEL AND SUBJECT DETAILS

Mouse models and husbandry—8-12-week-old female C57BL/6 (RRID: IMSR_JAX:000,664) were mated to male Flkswitch mice (Boyer et al., 2011, 2012; Epelman et al., 2014; Hoeffel et al., 2015; Beaudin, et al., 2016). Flkswitch mice were generated by crossing Flk2-Cre mice (Benz et al., 2008) to mTmG mice (Muzumdar et al., 2007) and gestation day was confirmed by the presence of a sperm plug. Flkswitch males were used because the Flk-Cre transgene is only transmitted through the Y chromosome. At gestation day 14.5, pregnant dams were weighed and treated with 20mg/kg Polyinosinic:polycytidylic acid (pIC) via intraperitoneal injection. For fetal timepoints, pregnant dams were euthanized, and fetuses were dissected from the uterine horn. Fetal liver GFP+ (Flkswitch) expression was confirmed by microscopy in fetuses or by peripheral blood analysis at postnatal timepoints, Postnatal day (P)14 and 8-week-old adult. For transplantation assays, FlkSwitch mice were used as donors for cell isolation and 8- to 12-week-old WT C57BL/6 were used as recipients. Sex of recipients was random and split evenly between male and female. All mice were maintained in the University of California, Merced vivarium according to Institutional Animal Care and Use Committee (IACUC)-approved protocols.

METHOD DETAILS

Cell isolation and identification by flow cytometry—Fetal livers were dissected and pipetted gently in staining media to form a single cell suspension. Adult and P14 BM cells isolated by dissecting long bones and using a mortar and pestle to gently crush bones in “staining media” (1XPBS, 2%FBS, .5mM EDTA) and bone marrow was extracted by gently pipetting. Cells were filtered through a 70uM filter. Cell populations were analyzed using a four-laser FACSAria III (BD Biosciences). Cells were sorted on The FACSAriaII (BD Biosciences) or III. All flow cytometric analysis was done using FlowJo. Hematopoietic and mature blood cell populations were identified as follows: Lineage dump or “Lin” for all fetal liver populations (CD3, CD4, CD5, CD8, CD19, Ter-119, Nk1.1, Gr-1, F4/80), Lin for adult bone marrow populations (CD3, CD4, CD5, CD8, Cd11b, CD19, Ter-119, Nk1.1, Gr-1, F4/80); LT-HSCs (Lin−, CD45+, cKit+, Sca1+, Flk2−, CD48−, CD150+), ST-HSCs (Lin−, CD45+, cKit+, Sca1+, Flk2−, CD48−, CD150−), Tom+ aHSCs, (Lin−, CD45+, cKit+, Sca1+, CD150+, Tom+), GFP + drHSCs (Lin−, CD45+, cKit+, Sca1+, CD150+, GFP+), MPP2 (Lin−, CD45+, cKit+, Sca1+, Flk2−, CD48+, CD150+), MPP3 (Lin−, CD45+, cKit+, Sca1+, Flk2−, CD48+ CD150−), MPP4 (Lin−, CD45+, CKit+, Sca1+, Flk2+, CD48+, CD150−), Granulocyte-Macrophage Progenitor “GM” (Lin− CKit+, CD41−, CD16/32+), Megakaryocyte Progenitor “MP”, Erythrocyte progenitor “EP”; Peritoneal Cavity: B1a (CD3−, F4/80-Gr1−, Ter119−, CD19+ CD5+), B1b (CD3−, F4/80-Gr1−,Ter119−, CD19+ CD5−, CD11b+), B2 (CD3−, F4/80-Gr1−,Ter119−, CD19+ CD5−, CD11b−); Splenic B cells: Marginal Zone B-cells “MZ” (CD3−, F4/80-Gr1−,Ter119−, IgM+, CD19+, CD21+ CD23−), Follicular Zone “FZ” B-cells (CD3−, F4/80-Gr1−,Ter119−, IgM+, CD19+, CD21− CD23+).

Proliferation of HSCs and MPPs—Fetal liver cells were processed into a single cell suspension and cKit-enriched using CD117 MicroBeads (Miltenyi Biotec, San Diego, CA, USA). The cKit-enriched population was stained with an antibody cocktail for surface

Author Manuscript Author Manuscript Author Manuscript Author Manuscript

markers of hematopoietic stem and progenitor cells. Cells were then fixed and permeabilized with the True-Nuclear Transcription buffer set (Biolegend) and then stained with Ki67-APC (Invitrogen, Carlsbad, CA, USA) and Hoescht 33,342 (Invitrogen).

Fluorescein-tagged pIC administration and imaging in the fetal liver—Pregnant C57BL/6 damns were injected at E14.5 with 10μg fluorescein-tagged pIC (InvivoGen) supplemented with untagged pIC to a final dose of 20mg/kg. Mice were sacrificed 24-h post injection and whole fetuses were placed in tissue molds, suspended over 2-methylbutane (Fisher Scientific), and imbedded in O.C.T. compound (Fisher Scientific). Embryos were frozen over dry ice and stored at −80°C. 20μm cryosections were collected at −20°C to −17°C and placed onto slides. Slides were allowed to dry in the dark at room temperature (RT) for 30 min prior to fixation with 10% formalin at RT for 15 min in the dark. Sections were washed 3X with 1X $PBS^{-/-}$ and dried overnight protected from light. Sections were stained with DAPI and coverslip was applied and secured before imaging. Fetal liver images were captured at 63X magnification using a Leica SP8 405-488-561-633 laser confocal microscope.

Culture of Tom+ HSC or GFP + drHSC to assess HSPC generation—E14.5 FL GFP + drHSCs and Tom+ HSCs were sorted form FlkSwitch embryos 2 h post *in vivo* saline or MIA treatment. 450 Tom+ HSCs or GFP + drHSCs were cultured at 37°C with 5% CO_2 in StemPro-34 SFM supplemented with 2mM L-Glutamine, 50 ng/mL SCF, 30 ng/mL Flt3L, 25 ng/mLTPO, and 100 ug/mL Primocin. Cells were harvested after 24 h, stained for HSPC surface cell markers, and analyzed using an Aurora Spectral Analyzer (Cytek). MPP3 and MPP4 populations were defined as Lin-cKit + Sca1+CD48+CD150-ESAM+ and cKit + Sca1+CD48+CD150-ESAM−, respectively (Beaudin et al., 2014).

Transplantation assays—Transplantations were performed by is sorting GFP + drHSCs and Tom+ HSCs from fetal liver. Recipient C57BL/6 mice (8-12 weeks) were lethally irradiated using 1000 cGy (split dose, Precision X-Rad 320). $5x10^6$ whole bone marrow cells from untreated age matched C57BL/6 and 200 sorted GFP + drHSCs or Tom+ HSCs wells were diluted in PBS and transplanted via retroorbital injection using a 1mL tuberculin syringe in a volume of 100–200 uL. Peripheral blood chimerism was determined in recipients by blood collection via cheek bleeds every 4 weeks for 16 weeks and cells were analyzed by flow cytometry using the LSRII (BD Biosciences). Long-term multilineage reconstitution (LTMR) was defined as chimerism >1% in all mature blood lineages. At 18 weeks, recipients were euthanized, and BM populations were assessed for chimerism by flow cytometry.

10x Chromium single-cell sequencing of HSPCs—Pregnant dams from C57BL/6 Flkswitch crosses were exposed to pIC or saline at E14.5. E15.5 fetal liver cells were pooled, cKit-enriched, and sorted for HSPCs (CD45+, Lin−, cKit + Sca1+). In order to get adequate cell numbers for analysis, at least 9 litters/condition (with 3–8 fetal livers/litter) were used for sorts. Sorted HSPCs were frozen at −80°C in FBS and 15% DMSO in cryovials until all samples were collected. Frozen cells were thawed in a 37°C water bath for 2-3 min and washed and resuspended in 10% FBS and assessed for 60-70% viability

Author Manuscript Author Manuscript Author Manuscript Author Manuscript

before processing. A sample library was generated using Chromium 10x V3 and run using NovaSeq.

scRNA-seq data pre-processing and quality control—Raw UMI-based data files were mapped against the mm10 reference genome using the scRNAseq tool from the bioinformatics pipe-line snakePipes, with the 10xV3 mode (Bhardwaj et al., 2019). In this tool, STARsolo was used to i) map, ii) UMI-deduplicate and iii) count reads, to create the BAM files and a Seurat object with the gene counts (Dobin et al., 2013). The quality of this data was checked by running Deeptools QC (Ramirez et al., 2016). After the preprocessing of data, R package Seurat was used to perform the single-cell RNA-seq analysis (Satija et al., 2015). The Seurat object was imported, and a cell filtering was performed, selecting the cells which i) contained more than 75,000 counts and ii) those that expressed above 2,000 genes to avoid empty droplets. Moreover, low-quality and dying cells with a percentage of mitochondrial mRNA higher than 20% were filtered out.

scRNA-seq data clustering and gene expression—A log-normalization and scaling of the data was applied prior to the linear dimension reduction with the Principal Component Analysis (PCA). After applying the JackStraw and Elbow plot procedures from Seurat, a clustering analysis was performed selecting the first 20 PCs, resulting in cell communities that were visualized with the Uniform Manifold Approximation and Projection (UMAP) technique (Becht et al., 2018). From those, three clusters were filtered out based on the doublets scoring calculated with the doubletCells function from scran package (Lun et al., 2016), the enrichment of LSK and LS-K signatures described previously (Klimmeck et al., 2014) applying the AddModuleScore function and the presence of differentiated cells markers, detected with the FindAllMarkers function (min.pct = 0, logfc.threshold = 0.15). A total of 23,505 cells distributed in 14 clusters were further analyzed, corresponding 11,977 and 11,528 cells to the pIC and Saline conditions, respectively. A heatmap with the expression of the top seven differentially expressed genes per cluster was performed with DoHeatmap function. The percentage of cells in each condition per cluster was visualized in a barplot, assessing the significance with Fisher tests. Cell cycle phase alignment was performed by calculating the G1 and G2M scores defined by the cyclone function from scran package, using default parameters (Scialdone et al., 2015). The enrichment of the eGFP, tdTomato signatures generated using reference data set from E14.5 fetal liver (Beaudin et al., 2016) and the also generated HSC and MPP gene expression signatures (Cabezas-Wallscheid et al., 2014) were depicted by the AddModuleScore function. The resulting enrichment was represented in the UMAP projection with the FeaturePlot function and in violin plots, calculating the significance per cluster with respect to all scores using a Wilcoxon signed rank test with one-sided alternative hypothesis. In the same way, the enrichment of the reactome database (reactome.org) pathways integral to cytokine, interferon and interleukin signaling in the immune system were represented individually in the single cell data as violin plots. Generated lists of cluster markers by the FindMarkers function (min.pct = 0.25, logfc.threshold = 0.25) were used for gene set enrichment analysis (GSEA) in the already published ranked set of differentially expressed genes between Tom+ HSC and GFP + drHSCs (Beaudin et al., 2016), using the GSEA and gseaplot2 functions (Yu, 2022).

Author Manuscript Author Manuscript Author Manuscript Author Manuscript

TLR3 and TLR3$^{KO/KO}$ experiments—8-12-week-old female C57BL/6 females were mated to C57BL/6 male mice and treated with 20mg/kg pIC or saline at E14.5. Females were sacrificed 2hrs later and FLs were harvested from embryos and processed as described above and. Cells were then stained using an HSPC antibody cocktail before being fixed and permeabilized with the True-Nuclear Transcription buffer set (Biolegend) and stained with TLR3-APC (Biolegend).

For TLR3 KO experiments, TLR3$^{KO/KO}$ female mice (RRID:IMSR_JAX:005,217) were mated to C57BL/6 males and treated with 20mg/kg pIC or saline at E14.5. Litters were aged to postnatal day (P)14, genotyped and sacrificed for BM HSPC analysis. Flow cytometric analysis was performed using an Aurora Spectral Analyzer (Cytek).

Inducible Mx-1 Cre lineage tracing—8-12-week-old female Ai9 reporter mice (RRID: IMSR JAX:007,909) were mated to male Mx1-Cre mice (RRID: IMSR JAX:003,556) and treated with 20mg/kg pIC or saline (control) at E14.5. After 1hr, 24 h, or 72 h post-MIA, FLs were processed as described above and cells were stained with antibody cocktails for HSPC, MkP (Lin−CD45+cKit + Sca1−CD150+CD41+), GMP (Lin−CD45+cKit + Sca1−CD150−FcγRIII/II+), Pre-GM (Lin−CD45+cKit + Sca1-CD150-FcγRIII/II-CD105−), Pre-MegE (Lin−CD45+cKit + Sca1−CD150+FcγRIII/II-CD105$^{lo/-}$), Pre CFU-E (Lin−CD45+cKit + Sca1-CD150+FcγRIII/II-CD105+), as defined by (Pronk et al., 2007), and B1a, and B1b populations. Flow cytometric analysis was performed using an Aurora Spectral Analyzer (Cytek). Frequency of label (%TdTomato+) was determined by taking the average background labeling in saline-treated controls and subtracting it from the frequency of label for each population in pIC-treated mice.

Quantitation of cytokines in fetal amniotic fluid and liver—Fetal amniotic fluid was collected from amniotic sacs using a 1 mL tuberculin syringe. Fetuses were dissected and individual fetal livers were homogenized and pelleted to collect supernatant. Supernatant was frozen at −80°C and samples were analyzed on an LSRII (BD Biosciences) following manufacturer recommendations using a custom LEGENDplex (Biolegend) bead-based immunoassay for the following cytokines: IL-23, IL-1α, IFNγ, TNF-α, IL-6, IL-1β, IL-10, IL-17A, IL-27, IFNβ, IFNα, and GM-CSF. Data were analyzed with LEGENDplex online analysis platform. https://legendplex.qognit.com/.

Isolation and stimulation of postnatal day 21 peritoneal B cells for IL-10 quantitation—Peritoneal washouts were performed by injecting 1mL of cold media+2% FBS into the peritoneal cavity (PEC) of P21 pups. Mice were shaken 10-15 times and media was pipetted out of the abdomen via an incision beneath the sternum. Multiple washes were performed (for a total of 3 washes) by adding more media through the incision under the sternum. Samples were filtered and pooled together for sorting. Cell populations were sorted and resuspended in sterile 1X RPMI +10% FBS +10ug/mL LPS and 25ng/mL of PMA or 1X RPMI +10% FBS as a control. Cells were plated at a concentration of 10,000 cells/well in a volume of 200mL of media and cultured for 24 h at 37°C with 5%CO2. After 24 h cells were pelleted, and supernatant was removed and stored at −80°C for further analysis. IL-10 samples were diluted to a factor of 1:4 and ELISA assay was performed using manufacturer's instructions (OptEIA, BD Biosciences).

Author Manuscript Author Manuscript Author Manuscript Author Manuscript

Peritoneal cavity wash and immunoglobulin quantitation with ELISA at postnatal day 14 or LEGENDplex in adults—Peritoneal washouts were performed by injecting 1mL of cold media into the PEC of P14 pups or 3mLs into adult mice. Small piece of skin was removed on the lower left quadrant of the mouse PEC and needle was inserted through peritoneum. 1mL (P14) or 3 mLs (adults) of media were injected and mice were shaken 10-15 times before the media was pipetted out of the abdomen via an incision beneath the sternum. Contaminated samples either because of intestinal leakage and/or visible blood in the supernatant were discarded. Sample was filtered with 70uM filter and 500ul of sample was taken for cellularity counts via hemocytometer and supernatant analysis. Supernatant was stored at −20°C until further analysis. For LEGENDplex assay, thawed supernatant samples were analyzed on a BD FACS Canto following manufacturer recommendations using LEGENDplex Immunoglobulin Isotyping Panel (Biolegend) bead-based immunoassay. Data were analyzed with LEGENDplex online analysis platform https://legendplex.qognit.com/.

MaxiSorp plates were coated with 50ul Ig capture antibody (2ug/mL) or Phosphorylcholine-BSA (PC-BSA) (10ug/mL) for anti-PC IgM ELISAs and incubated for 2 h at 37C. Plates were washed 3 times and blocked with 1X PBS +0.5% Tween 20 + 0.5% BSA and incubated for 1 h at RT. Plates were washed and samples and standards (2-fold serial dilution) were added and incubated for 2 h at RT. Plates were washed and 50ul of appropriate detection (1:7000 dilution, or 1:2000 dilution for PC ELISA) was added to wells and incubated for 1 h at RT. Plates were washed and 50ul TMB substrate was added to all wells and incubated for ~15 min at RT. 50ul of 1N sulfuric acid was added to stop the TMB reaction and plate was read at 450nm immediately following the addition of stop solution. PEC samples were normalized to cellularity (Total concentration/Total PEC cellularity).

QUANTIFICATION AND STATISTICAL ANALYSIS

Prism v8.0 (GraphPad Software, San Diego, CA, USA) was used to perform statistical tests. Transplantation assays were randomized across age, sex, and cage for any given experiment. Investigator was blinded to treatment during preparation and analysis of samples. Statistically significant differences between groups with similar variance as determined by the SEM and SD were assessed by either un-paired two-tailed t-tests for parametric data, or Mann–Whitney tests for non-parametric data. two-way ANOVA with Tukey's multiple comparisons was used for comparison of GFP + drHSC and Tom+ HSC under pIC or saline conditions. p values were calculated and are indicated as follows: *$p \leq 0.05$; **$p \leq 0.01$; ***$p \leq 0.001$; ****$p \leq 0.0001$. Sample sizes are indicated in each figure and unless otherwise noted, all experiments were performed in at least three independent replicates. All statistical details (including N and p values) for individual experiments can be found in figure legends.

Supplementary Material

Refer to Web version on PubMed Central for supplementary material.

Author Manuscript Author Manuscript Author Manuscript Author Manuscript

ACKNOWLEDGMENTS

We thank Dr. T. Boehm for the Flt3-Cre mice, David Gravano and the UC Merced Stem Cell Instrumentation Foundry, James Marvin and the University of Utah Flow Cytometry Core, Bari Nazario for flow cytometry support, and Jasmine Posada for technical assistance. We thank Dr. Robert Signer for thoughtful comments on the manuscript. This work was supported by an NIH/NHLBI award K01HL130753 to A.E.B., the Pew Biomedical Scholars award to A.E.B., and the Hellman Fellows Award to A.E.B.; NIH/NIDDK R01DK100917 to E.C.F.; and Max Planck Society and the ERC-Stg-2017 (Vi-tASTEM) Research to N.C.-W. Additional support included CIRM facilities awards CL1-00506 and FA1-00617 to UCSC and the DoD Research and Education Program for HBCU/MSI Instrumentation Grant W911NF1910529, National Center for Research Resources of the NIH award number 1S10RR026802-01, and NIH Shared Instrumentation Grant 1S10OD010786-01 to the DNA Technologies and Expression Analysis Core at the UC Davis Genome Center. D.A.L. is supported by NIH/NICHD training grant T32HD007491. G.E.H. is supported by Howard Hughes Medical Institute Gilliam Fellowship (GT11560). A.E.B. is the recipient of NIH/NHLBI R01HL147081.

REFERENCES

Ander SE, Diamond MS, and Coyne CB (2019). Immune responses at the maternal-fetal interface. Sci. Immunol 4, eaat6114. 10.1126/sciimmunol.aat6114. [PubMed: 30635356]

Apostol AC, Jensen KDC, and Beaudin AE (2020). Training the fetal immune system through maternal inflammation-A layered hygiene hypothesis. Front. Immunol 11, 123. 10.3389/fimmu.2020.00123. [PubMed: 32117273]

Baldridge MT, King KY, Boles NC, Weksberg DC, and Goodell MA (2010). Quiescent haematopoietic stem cells are activated by IFN-gamma in response to chronic infection. Nature 465, 793–797. 10.1038/nature09135. [PubMed: 20535209]

Baumgarth N (2011). The double life of a B-1 cell: self-reactivity selects for protective effector functions. Nat. Rev. Immunol 11, 34–46. 10.1038/nri2901. [PubMed: 21151033]

Baumgarth N (2021). The shaping of a B cell pool maximally responsive to infections. Annu. Rev. Immunol 39, 103–129. 10.1146/annurev-immunol-042718-041238. [PubMed: 33472004]

Beaudin AE, Boyer SW, and Forsberg EC (2014). Flk2/Flt3 promotes both myeloid and lymphoid development by expanding non-self-renewing multipotent hematopoietic progenitor cells. Exp. Hematol 42, 218–229.e4. 10.1016/j.exphem.2013.11.013. [PubMed: 24333663]

Beaudin AE, Boyer SW, Perez-Cunningham J, Hernandez GE, Derderian SC, Jujjavarapu C, Aaserude E, MacKenzie T, and Forsberg EC (2016). A transient developmental hematopoietic stem cell gives rise to innate-like B and T cells. Cell Stem Cell 19, 768–783. 10.1016/j.stem.2016.08.013. [PubMed: 27666010]

Beaudin AE, and Forsberg EC (2016). To B1a or not to B1a: do hematopoietic stem cells contribute to tissue-resident immune cells? Blood 128, 2765–2769. 10.1182/blood-2016-10-697813. [PubMed: 27799163]

Becht E, McInnes L, Healy J, Dutertre CA, Kwok IWH, Ng LG, Ginhoux F, and Newell EW (2018). Dimensionality reduction for visualizing single-cell data using UMAP. Nat. Biotechnol 37, 38–44. 10.1038/nbt.4314.

Beerman I, Bhattacharya D, Zandi S, Sigvardsson M, Weissman IL, Bryder D, and Rossi DJ (2010). Functionally distinct hematopoietic stem cells modulate hematopoietic lineage potential during aging by a mechanism of clonal expansion. Proc. Natl. Acad. Sci. USA 107, 5465–5470. 10.1073/pnas.1000834107. [PubMed: 20304793]

Benz C, Copley MR, Kent DG, Wohrer S, Cortes A, Aghaeepour N, Ma E, Mader H, Rowe K, Day C, et al. (2012). Hematopoietic stem cell subtypes expand differentially during development and display distinct lymphopoietic programs. Cell Stem Cell 10, 273–283. 10.1016/j.stem.2012.02.007. [PubMed: 22385655]

Benz C, Martins VC, Radtke F, and Bleul CC (2008). The stream of precursors that colonizes the thymus proceeds selectively through the early T lineage precursor stage of T cell development. J. Exp. Med 205, 1187–1199. 10.1084/jem.20072168. [PubMed: 18458114]

Bhardwaj V, Heyne S, Sikora K, Rabbani L, Rauer M, Kilpert F, Richter AS, Ryan DP, and Manke T (2019). snakePipes: facilitating flexible, scalable and integrative epigenomic analysis. Bioinformatics 35, 4757–4759. 10.1093/bioinformatics/btz436. [PubMed: 31134269]

Author Manuscript Author Manuscript Author Manuscript Author Manuscript

Böiers C, Carrelha J, Lutteropp M, Luc S, Green JCA, Azzoni E, Woll PS, Mead AJ, Hultquist A, Swiers G, et al. (2013). Lymphomyeloid contribution of an immune-restricted progenitor emerging prior to definitive hematopoietic stem cells. Cell Stem Cell 13, 535–548. 10.1016/j.stem.2013.08.012. [PubMed: 24054998]

Boyer SW, Beaudin AE, and Forsberg EC (2012). Mapping stem cell differentiation pathways from hematopoietic stem cells using Flk2/Flt3L lineage tracing. Cell Cycle 11, 3180–3188. [PubMed: 22895180]

Boyer SW, Schroeder AV, Smith-Berdan S, and Forsberg EC (2011). All hematopoietic cells develop from hematopoietic stem cells through Flk2/Flt3-positive progenitor cells. Cell Stem Cell 9, 64–73. 10.1016/j.stem.2011.04.021. [PubMed: 21726834]

Busch K, Klapproth K, Barile M, Flossdorf M, Holland-Letz T, Schlenner SM, Reth M, Höfer T, and Rodewald HR (2015). Fundamental properties of unperturbed haematopoiesis from stem cells in vivo. Nature 518, 542–546. 10.1038/nature14242. [PubMed: 25686605]

Cabezas-Wallscheid N, Klimmeck D, Hansson J, Lipka DB, Reyes A, Wang Q, Weichenhan D, Lier A, von Paleske L, Renders S, et al. (2014). Identification of regulatory networks in HSCs and their immediate progeny via integrated proteome, transcriptome, and DNA methylome analysis. Cell Stem Cell 15, 507–522. 10.1016/j.stem.2014.07.005. [PubMed: 25158935]

Chavakis T, Mitroulis I, and Hajishengallis G (2019). Hematopoietic progenitor cells as integrative hubs for adaptation to and fine-tuning of inflammation. Nat. Immunol 20, 802–811. 10.1038/s41590-019-0402-5. [PubMed: 31213716]

Crisan M, Solaimani Kartalaei P, Neagu A, Karkanpouna S, Yamada-Inagawa T, Purini C, Vink CS, van der Linden R, van Ijcken W, Chuva de Sousa Lopes SM, et al. (2016). BMP and hedgehog regulate distinct AGM hematopoietic stem cells ex vivo. Stem Cell Rep. 6, 383–395. 10.1016/j.stemcr.2016.01.016.

Dobin A, Davis CA, Schlesinger F, Drenkow J, Zaleski C, Jha S, Batut P, Chaisson M, and Gingeras TR (2013). STAR: ultrafast universal RNA-seq aligner. Bioinformatics 29, 15–21. 10.1093/bioinformatics/bts635. [PubMed: 23104886]

Epelman S, Lavine KJ, Beaudin AE, Sojka DK, Carrero JA, Calderon B, Brija T, Gautier EL, Ivanov S, Satpathy AT, et al. (2014). Embryonic and adult-derived resident cardiac macrophages are maintained through distinct mechanisms at steady state and during inflammation. Immunity 40, 91–104. [PubMed: 24439267]

Espin-Palazon R, Weijts B, Mulero V, and Traver D (2018). Proinflammatory signals as fuel for the fire of hematopoietic stem cell emergence. Trends Cell Biol. 28, 58–66. 10.1016/j.tcb.2017.08.003. [PubMed: 28882414]

Esplin BL, Shimazu T, Welner RS, Garrett KP, Nie L, Zhang Q, Humphrey MB, Yang Q, Borghesi LA, and Kincade PW (2011). Chronic exposure to a TLR ligand injures hematopoietic stem cells. J. Immunol 186, 5367–5375. 10.4049/jimmunol.1003438. [PubMed: 21441445]

Essers MAG, Offner S, Blanco-Bose WE, Waibler Z, Kalinke U, Duchosal MA, and Trumpp A (2009). IFNalpha activates dormant haematopoietic stem cells in vivo. Nature 458, 904–908. 10.1038/nature07815. [PubMed: 19212321]

Ficara F, Murphy MJ, Lin M, and Cleary ML (2008). Pbx1 regulates self-renewal of long-term hematopoietic stem cells by maintaining their quiescence. Cell Stem Cell 2, 484–496. 10.1016/j.stem.2008.03.004. [PubMed: 18462698]

Furusawa J.i., Mizoguchi I, Chiba Y, Hisada M, Kobayashi F, Yoshida H, Nakae S, Tsuchida A, Matsumoto T, Ema H, et al. (2016). Promotion of expansion and differentiation of hematopoietic stem cells by interleukin-27 into myeloid progenitors to control infection in emergency myelopoiesis. PLoS Pathog. 12, e1005507. 10.1371/journal.ppat.1005507. [PubMed: 26991425]

Gazit R, Garrison BS, Rao TN, Shay T, Costello J, Ericson J, Kim F, Collins JJ, Regev A, Wagers AJ, et al. (2013). Transcriptome analysis identifies regulators of hematopoietic stem and progenitor cells. Stem Cell Rep. 1, 266–280. 10.1016/j.stemcr.2013.07.004.

Gekas C, and Graf T (2013). CD41 expression marks myeloid-biased adult hematopoietic stem cells and increases with age. Blood 121, 4463–4472. 10.1182/blood-2012-09-457929. [PubMed: 23564910]

Author Manuscript Author Manuscript Author Manuscript Author Manuscript

Guo XL, Chu L, Ke F, Mu LL, Li Z, Cai JJ, Li HF, and Hong DL (2017). Recipient bone marrow assimilates the myeloid/lymphoid reconstitution of distinct fetal hematopoietic stem cells. Oncotarget 8, 108981–108988. 10.18632/oncotarget.22479. [PubMed: 29312584]

Haas S, Hansson J, Klimmeck D, Loeffler D, Velten L, Uckelmann H, Wurzer S, Prendergast ÁM, Schnell A, Hexel K, et al. (2015). Inflammation-induced emergency megakaryopoiesis driven by hematopoietic stem cell-like megakaryocyte progenitors. Cell Stem Cell 17, 422–434. 10.1016/j.stem.2015.07.007. [PubMed: 26299573]

Herzenberg LA (1989). Toward a layered immune system. Cell 59, 953–954. [PubMed: 2688900]

Hoeffel G, Chen J, Lavin Y, Low D, Almeida FF, See P, Beaudin AE, Lum J, Low I, Forsberg EC, et al. (2015). C-Myb+ Erythro-Myeloid Progenitor-Derived Fetal Monocytes Give Rise to Adult Tissue-Resident Macrophages. Immunity 42, 665–678. [PubMed: 25902481]

Hsiao EY, McBride SW, Chow J, Mazmanian SK, and Patterson PH (2012). Modeling an autism risk factor in mice leads to permanent immune dysregulation. Proc. Natl. Acad. Sci. USA 109, 12776–12781. 10.1073/pnas.1202556109. [PubMed: 22802640]

Kaufmann E, Sanz J, Dunn JL, Khan N, Mendonça LE, Pacis A, Tzelepis F, Pernet E, Dumaine A, Grenier JC, et al. (2018). BCG educates hematopoietic stem cells to generate protective innate immunity against. Cell 172, 176–190.e19. 10.1016/j.cell.2017.12.031. [PubMed: 29328912]

King KY, and Goodell MA (2011). Inflammatory modulation of HSCs: viewing the HSC as a foundation for the immune response. Nat. Rev. Immunol 11, 685–692. 10.1038/nri3062. [PubMed: 21904387]

Klimmeck D, Cabezas-Wallscheid N, Reyes A, von Paleske L, Renders S, Hansson J, Krijgsveld J, Huber W, and Trumpp A (2014). Transcriptome-wide profiling and posttranscriptional analysis of hematopoietic stem/progenitor cell differentiation toward myeloid commitment. Stem Cell Rep. 3, 858–875. 10.1016/j.stemcr.2014.08.012.

Li Y, Kong W, Yang W, Patel RM, Casey EB, Okeyo-Owuor T, White JM, Porter SN, Morris SA, and Magee JA (2020). Single-cell analysis of neonatal HSC ontogeny reveals gradual and uncoordinated transcriptional reprogramming that begins before birth. Cell Stem Cell 27, 732–747.e7. 10.1016/j.stem.2020.08.001. [PubMed: 32822583]

Love MI, Huber W, and Anders S (2014). Moderated estimation of fold change and dispersion for RNA-seq data with DESeq2. Genome Biology. 10.1186/s13059-014-0550-8.

Luckey CJ, Bhattacharya D, Goldrath AW, Weissman IL, Benoist C, and Mathis D (2006). Memory T and memory B cells share a transcriptional program of self-renewal with long-term hematopoietic stem cells. Proc. Natl. Acad. Sci. USA 103, 3304–3309. 10.1073/pnas.0511137103. [PubMed: 16492737]

Lun ATL, McCarthy DJ, and Marioni JC (2016).A step-by-step workflow for low-level analysis of single-cell RNA-seq data with Bioconductor. F1000Res. 5, 2122. 10.12688/f1000research.9501.2. [PubMed: 27909575]

Mandal M, Donnelly R, Elkabes S, Zhang P, Davini D, David BT, and Ponzio NM (2013). Maternal immune stimulation during pregnancy shapes the immunological phenotype of offspring. Brain Behav. Immun 33, 33–45. 10.1016/j.bbi.2013.04.012. [PubMed: 23643646]

Mandal M, Marzouk AC, Donnelly R, and Ponzio NM (2010). Preferential development of Th17 cells in offspring of immunostimulated pregnant mice. J. Reprod. Immunol 87, 97–100. 10.1016/j.jri.2010.06.156. [PubMed: 20727596]

Mandal M, Marzouk AC, Donnelly R, and Ponzio NM (2011). Maternal immune stimulation during pregnancy affects adaptive immunity in offspring to promote development of TH17 cells. Brain Behav. Immun 25, 863–871. 10.1016/j.bbi.2010.09.011. [PubMed: 20854892]

Mann M, Mehta A, de Boer CG, Kowalczyk MS, Lee K, Haldeman P, Rogel N, Knecht AR, Farouq D, Regev A, and Baltimore D (2018). Heterogeneous responses of hematopoietic stem cells to inflammatory stimuli are altered with age. Cell Rep. 25, 2992–3005.e5. 10.1016/j.celrep.2018.11.056. [PubMed: 30540934]

Matatall KA, Shen CC, Challen GA, and King KY (2014). Type II interferon promotes differentiation of myeloid-biased hematopoietic stem cells. Stem Cell. 32, 3023–3030. 10.1002/stem.1799.

Author Manuscript Author Manuscript Author Manuscript Author Manuscript

Meyer U, Feldon J, and Fatemi SH (2009). In-vivo rodent models for the experimental investigation of prenatal immune activation effects in neurodevelopmental brain disorders. Neurosci. Biobehav. Rev 33, 1061–1079. 10.1016/j.neubiorev.2009.05.001. [PubMed: 19442688]

Mitroulis I, Ruppova K, Wang B, Chen LS, Grzybek M, Grinenko T, Eugster A,Troullinaki M, Palladini A, Kourtzelis I, et al. (2018). Modulation of myelopoiesis progenitors is an integral component of trained immunity. Cell 172, 147–161.e12. 10.1016/j.cell.2017.11.034. [PubMed: 29328910]

Montecino-Rodriguez E, and Dorshkind K (2006). New perspectives in B-1 B cell development and function. Trends Immunol. 27, 428–433. 10.1016/j.it.2006.07.005. [PubMed: 16861037]

Moran-Crusio K, Reavie L, Shih A, Abdel-Wahab O, Ndiaye-Lobry D, Lobry C, Figueroa ME, Vasanthakumar A, Patel J, Zhao X, et al. (2011). Tet2 loss leads to increased hematopoietic stem cell self-renewal and myeloid transformation. Cancer Cell 20, 11–24. 10.1016/j.ccr.2011.06.001. [PubMed: 21723200]

Muzumdar MD, Tasic B, Miyamichi K, Li L, and Luo L (2007). A global double-fluorescent Cre reporter mouse. Genesis 45, 593–605. 10.1002/dvg.20335. [PubMed: 17868096]

Nagai Y, Garrett KP, Ohta S, Bahrun U, Kouro T, Akira S, Takatsu K, and Kincade PW (2006). Toll-like receptors on hematopoietic progenitor cells stimulate innate immune system replenishment. Immunity 24, 801–812. 10.1016/j.immuni.2006.04.008. [PubMed: 16782035]

Pietras EM (2017). Inflammation: a key regulator of hematopoietic stem cell fate in health and disease. Blood 130, 1693–1698. 10.1182/blood-2017-06-780882. [PubMed: 28874349]

Pietras EM, Mirantes-Barbeito C, Fong S, Loeffler D, Kovtonyuk LV, Zhang S, Lakshminarasimhan R, Chin CP, Techner JM, Will B, et al. (2016). Chronic interleukin-1 exposure drives haematopoietic stem cells towards precocious myeloid differentiation at the expense of self-renewal. Nat. Cell Biol 18, 607–618. 10.1038/ncb3346. [PubMed: 27111842]

Pietras EM, Reynaud D, Kang YA, Carlin D, Calero-Nieto FJ, Leavitt AD, Stuart JM, Göttgens B, and Passegué E (2015). Functionally distinct subsets of lineage-biased multipotent progenitors control blood production in normal and regenerative conditions. Cell Stem Cell 17, 35–46. 10.1016/j.stem.2015.05.003. [PubMed: 26095048]

Pronk CJH, Rossi DJ, Månsson R, Attema JL, Norddahl GL, Chan CKF, Sigvardsson M, Weissman IL, and Bryder D (2007). Elucidation of the phenotypic, functional, and molecular topography of a myeloerythroid progenitor cell hierarchy. Cell Stem Cell 1, 428–442. 10.1016/j.stem.2007.07.005. [PubMed: 18371379]

Ramírez F, Ryan DP, Grüning B, Bhardwaj V, Kilpert F, Richter AS, Heyne S, Dündar F, and Manke T (2016). deepTools2: a next generation web server for deep-sequencing data analysis. Nucleic Acids Res. 44, W160–W165. 10.1093/nar/gkw257. [PubMed: 27079975]

Romagnoli C, Frezza S, Cingolani A, De Luca A, Puopolo M, De Carolis MP, Vento G, Antinori A, and Tortorolo G (2001). Plasma levels of interleukin-6 and interleukin-10 in preterm neonates evaluated for sepsis. Eur. J. Pediatr 160, 345–350. 10.1007/pl00008445. [PubMed: 11421413]

Satija R, Farrell JA, Gennert D, Schier AF, and Regev A (2015). Spatial reconstruction of single-cell gene expression data. Nat. Biotechnol 33, 495–502. 10.1038/nbt.3192. [PubMed: 25867923]

Schuettpelz LG, and Link DC (2013). Regulation of hematopoietic stem cell activity by inflammation. Front. Immunol 4, 204. 10.3389/fimmu.2013.00204. [PubMed: 23882270]

Scialdone A, Natarajan KN, Saraiva LR, Proserpio V, Teichmann SA, Stegle O, Marioni JC, and Buettner F (2015). Computational assignment of cell-cycle stage from single-cell transcriptome data. Methods 85, 54–61. [PubMed: 26142758]

Smith FL, and Baumgarth N (2019). B-1 cell responses to infections. Curr. Opin. Immunol 57, 23–31. 10.1016/j.coi.2018.12.001. [PubMed: 30685692]

Staber PB, Zhang P, Ye M, Welner RS, Nombela-Arrieta C, Bach C, Kerenyi M, Bartholdy BA, Zhang H, Alberich-Jordà M, et al. (2013). Sustained PU.1 levels balance cell-cycle regulators to prevent exhaustion of adult hematopoietic stem cells. Mol. Cell 49, 934–946. 10.1016/j.molcel.2013.01.007. [PubMed: 23395001]

Staeheli P, Danielson P, Haller O, and Sutcliffe JG (1986).Transcriptional activation of the mouse Mx gene by type I interferon. Mol. Cell Biol 6, 4770–4774. 10.1128/mcb.6.12.4770. [PubMed: 3796617]

Author Manuscript Author Manuscript Author Manuscript Author Manuscript

Takizawa H, Boettcher S, and Manz MG (2012). Demand-adapted regulation of early hematopoiesis in infection and inflammation. Blood 119, 2991–3002. [PubMed: 22246037]

Takizawa H, Fritsch K, Kovtonyuk LV, Saito Y, Yakkala C, Jacobs K, Ahuja AK, Lopes M, Hausmann A, Hardt WD, et al. (2017). Pathogen-induced TLR4-TRIF innate immune signaling in hematopoietic stem cells promotes proliferation but reduces competitive fitness. Cell Stem Cell 21, 225–240.e5. 10.1016/j.stem.2017.06.013. [PubMed: 28736216]

Yamashita M, and Passegué E (2019). TNF-A coordinates hematopoietic stem cell survival and myeloid regeneration. Cell Stem Cell 25, 357–372.e7. 10.1016/j.stem.2019.05.019. [PubMed: 31230859]

Ye Q, Du LZ, Shao WX, and Shang SQ (2017). Utility of cytokines to predict neonatal sepsis. Pediatr. Res 81, 616–621. 10.1038/pr.2016.267. [PubMed: 27997530]

Yu G enrichplot: Visualization of Functional Enrichment Result. R package version 1.18.0 https://yulab-smu.top/biomedical-knowledge-mining-book/.

Author Manuscript Author Manuscript Author Manuscript Author Manuscript

Highlights

- Fetal hematopoietic progenitors respond to prenatal inflammation
- Prenatal inflammation induces a lymphoid-biased response during development
- Prenatal inflammation shapes postnatal immune output at the hematopoietic stem cell level
- Prenatal inflammation causes expansion and hyperactivation of innate-like lymphocytes

Author Manuscript Author Manuscript Author Manuscript Author Manuscript

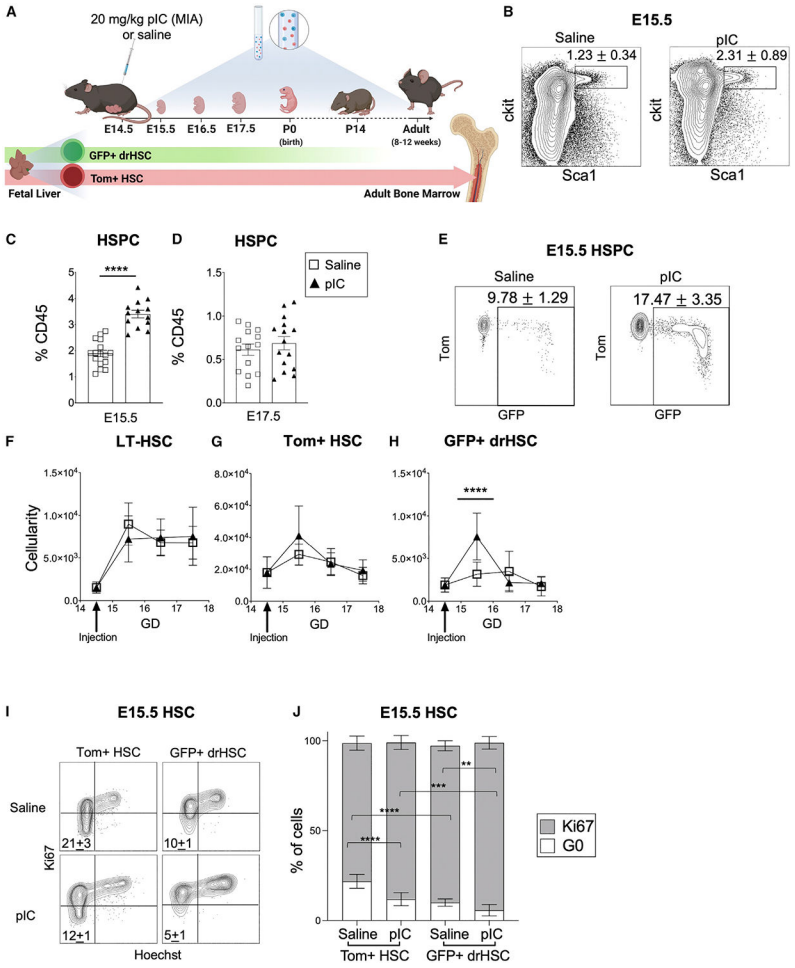

Figure 1. Fetal HSPCs respond to prenatal inflammation induced by MIA

(A) Timeline of MIA induction and analysis of fetal liver (FL) hematopoiesis. Pregnant WT dams mated to FlkSwitch males were intraperitoneally (i.p.) injected with 20 mg/kg polyinosinic-polycytidylic acid (pIC) at E14.5. Both Tom+ HSCs and GFP+ drHSCs are present in the FL during development, but only Tom+ HSCs persist into the adult bone marrow (BM). Image created with Biorender.com.

(B) Representative fluorescence-activated cell sorting (FACS) plots of the HSPC compartment (Live, Lin−, CD45+, cKit+, Sca1+) at E15.5, 1 day after pIC or saline induction. Numbers indicate average frequency ± SD.

(C and D) Frequency of HSPCs (as %CD45+ cells) in FL at E15.5 (C) and E17.5 (D). Data represent average ± SEM.

(E) Representative FACS plots showing frequency of GFP+ cells within the HSPC compartment at E15.5 in mice described in Figure 1B. Data represent frequency ± SD.

(F–H) Quantification of long-term HSCs (F; LT-HSCs; LSK Flk2− CD150+ CD48−), Tom+ HSCs (G; LSK CD150+ Tom+), and GFP+ drHSCs (H; LSK CD150+ GFP+) across gestation days (GD) following maternal injection of pIC or saline. For all above experiments, N = 3–6 pups/litter representing at least three litters/condition. Data represent average ± SEM.

Author Manuscript Author Manuscript Author Manuscript Author Manuscript

(I) Representative FACS plots measuring proliferation by Ki67 expression and Hoechst staining of Tom+ HSC and GFP+ drHSCs after saline or pIC. N = 3 litters/condition, two or three pups/litter. Data represent frequency ± SD.
(J) Quantification of Ki67 expression at E15.5 in both Tom+ HSCs and GFP+ drHSCs following pIC or saline in mice described in Figure 1L. Bars represent average ± SD.

Author Manuscript Author Manuscript Author Manuscript Author Manuscript

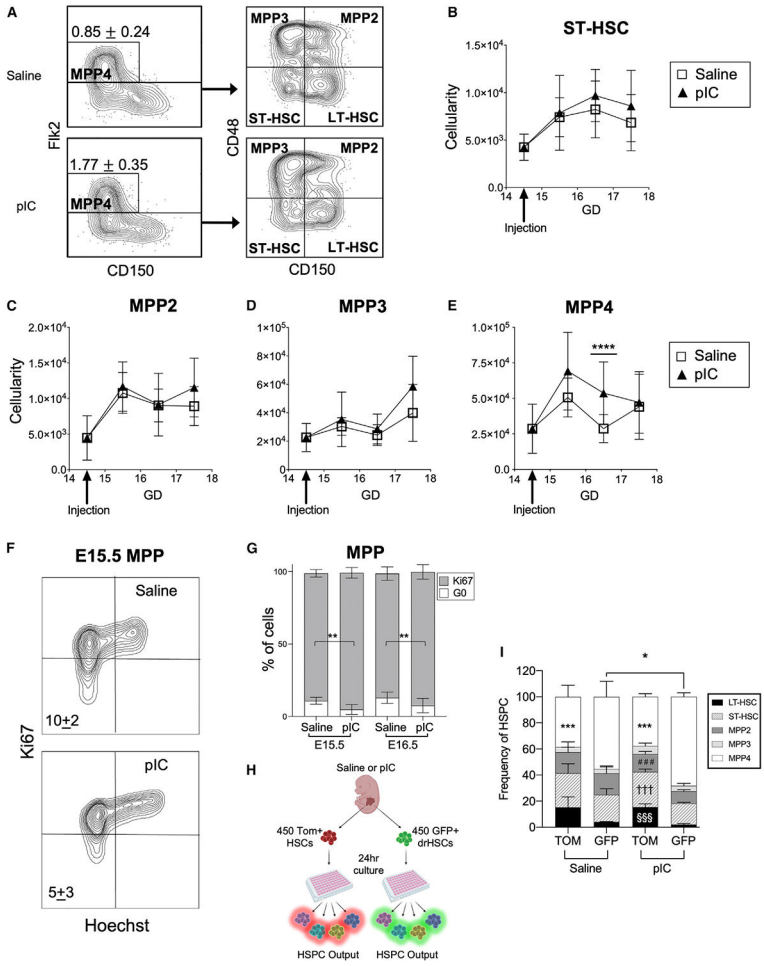

Figure 2. Lymphoid-biased fetal progenitors expand in response to prenatal inflammation induced by MIA

(A) Representative FACS plots of the HSPC compartment at E15.5. Numbers indicate average frequency ± SD of MPP4s in MIA and saline conditions. Data represent at least three to six pups/litter and three litters/condition.

(B–E) Cellularity of short-term HSCs (ST-HSC) (B), MPP2s (C), MPP3s (D), and MPP4s (E) across GD 15–17 following MIA or saline. Data represent average ±SEM for at least three to six pups/litter and three litters/condition.

(F) Representative flow cytometric plots of Ki67 expression and Hoechst staining in MPP (CD150− HSPC) populations after MIA or saline. Data represent average ± SD. N ≥ 3 litters/condition, three to six pups/litter.

(G) Quantification of Ki67 expression in MPPs (CD150− HSPC) from GD 15–17 after MIA or saline treatment. Data represent average ± SD for at least three to six pups/litter for three litters/condition at each time point.

(H) Schematic for *ex vivo* culture experiments. Two hours post *in vivo* treatment with pIC or saline, 450 Tom+ HSCs or GFP+ drHSCs were sorted and cultured. HSPC output was analyzed 24 h later. N = 2 or more independent experiments with three technical replicates.

(I) Frequency of HSPC subsets generated from cultured saline or pIC-treated Tom+ HSCs or GFP+ drHSCs. Data represent average ±SD from at least two independent experiments

performed in triplicate. Significance indicated within bars represents statistically significant differences between TOM+ or GFP+ LT-HSCs (§), ST-HSCs (†), MPP2s (#), or MPP4s (*) within each treatment condition. Overhead significance bracket indicates statistically significant differences between saline and pIC conditions for Tom+ HSCs or GFP drHSCs, respectively. Only GFP+ MPP4s (*) were significantly different between saline and pIC conditions. *$p \leq 0.05$; ***, §§§, †††, ###$p \leq 0.001$.

Author Manuscript Author Manuscript Author Manuscript Author Manuscript

Author Manuscript Author Manuscript Author Manuscript Author Manuscript

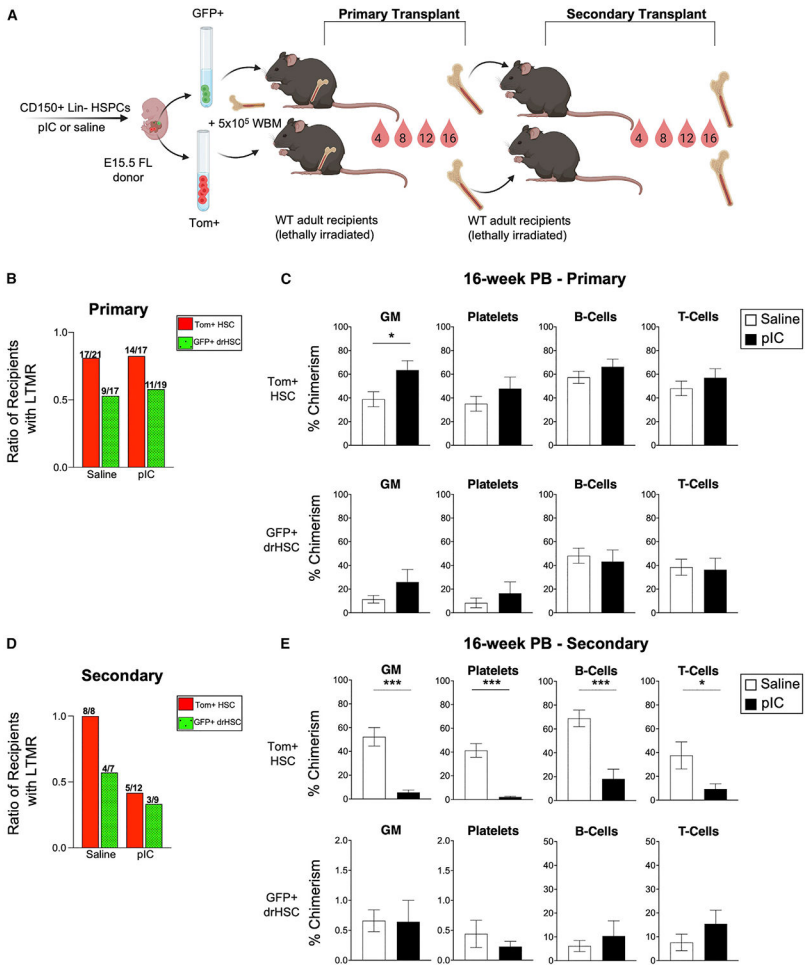

Figure 3. Prenatal inflammation induced by MIA causes persistent changes to fetal HSCs upon transplantation

(A) Schematic of transplantation approach. After MIA at E14.5, E15.5 Tom+ HSCs or GFP+ drHSCs were sorted and transplanted into lethally irradiated C57BL/6 hosts (200 HSCs/host) along with 5×10^5 whole bone marrow (WBM) cells. Peripheral blood (PB) was analyzed every 4 weeks until week 16. Image created with Biorender.com.

(B) The ratio of recipients with long-term multilineage reconstitution (LTMR) from transplants of Tom+ HSCs (red bar) and GFP+ drHSCs (patterned green bar) from pIC and saline-treated litters. N as indicated by numbers above bars, 13–19 recipients/condition.

(C) PB chimerism at 16 weeks of granulocyte/macrophage (GM), platelets (Plt), B cells, and T cells in recipients of Tom+ HSCs or GFP+ drHSCs, from same mice indicated in Figure 3B. Data represent average ± SEM.

(D) The ratio of recipients with LTMR from secondary transplants of 5×10^6 WBM cells from primary recipients of Tom+ HSCs (red bar) and GFP+ drHSCs (patterned green bar) from mice indicated in (B). N as indicated by numbers above bars, 7–12 recipients/condition.

(E) PB chimerism at 16 weeks of GM, Plt, B cells, and T cells in secondary recipients described in (D). Data represent average ± SEM.

Author Manuscript Author Manuscript Author Manuscript Author Manuscript

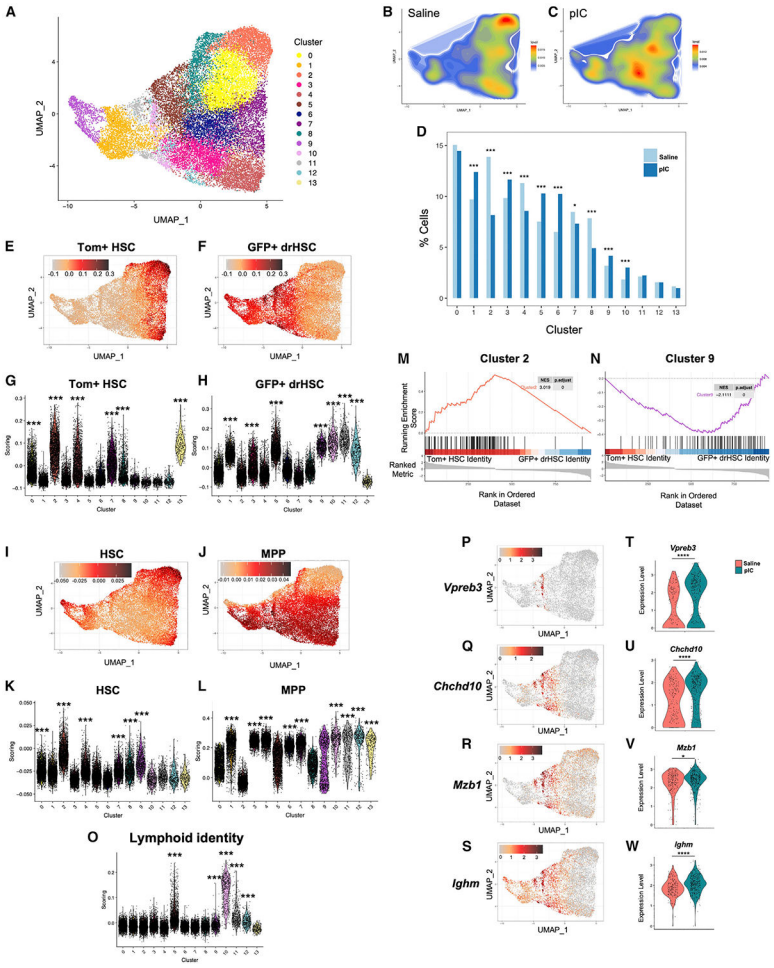

Figure 4. Prenatal inflammation induces distinct molecular changes in fetal HSCs

(A) Uniform Manifold Approximation and Projection (UMAP) plot of single-cell RNA sequencing showing 14 identified clusters from sorted E15.5 FL Tom+ or GFP+ HSPCs (Lin−CD45+cKit+Sca1+) following pIC or saline treatment at E14.5. N = 3 independent experiments.

(B and C) Representative density plots of clusters shown in 4A under saline (B) or pIC (C) conditions.

(D) Changes in percentage of cells in each cluster, visualized in a bar plot, in response to pIC or saline. Significance determined using Fisher tests.

(E and F) UMAP plots showing enrichment scoring for Tom+ HSC (E) or GFP+ drHSC (F) signatures across clusters using reference bulk dataset (Beaudin et al., 2016). Color bar indicates the enrichment scoring assessed by the AddModuleScore function.

(G and H) Violin plots showing enrichment scoring for Tom+ HSC (G) or GFP+ drHSC (H) signatures across clusters using a reference population dataset (Beaudin et al., 2016). Wilcoxon signed rank test with respect to background.

(I and J) UMAP plots showing enrichment scoring for HSC (I) or MPP (J) signatures across clusters using reference bulk dataset (Cabezas-Wallscheid et al., 2014). Color bar indicates the enrichment scoring assessed by the AddModuleScore function.

Author Manuscript Author Manuscript Author Manuscript Author Manuscript

(K and L) Violin plots showing enrichment scoring for adult HSC (K) or MPP (L) signatures across clusters using a reference population dataset (Cabezas-Wallscheid et al., 2014). Wilcoxon signed rank test with respect to background.

(M and N) Gene set enrichment analysis (GSEA) of Cluster C2 (M) and C9 (N) markers identified by FindMarkers function in a ranked set of differentially expressed genes between Tom+ HSC and GFP+ drHSCs (Beaudin et al., 2016).

(O) Violin plots showing enrichment scoring for lymphoid gene signature across all clusters using a reference population dataset (Cabezas-Wallscheid et al., 2014). Wilcoxon signed rank test with respect to background.

(P–S) UMAP plots showing gene expression levels of *Vpreb3* (P), *Chchd10* (Q), *Mzb1* (R), and *Ighm* (S) under saline control conditions.

(T and W) Violin plots comparing expression of C10 markers under saline and pIC conditions. Wilcoxon signed rank test.

Author Manuscript Author Manuscript Author Manuscript Author Manuscript

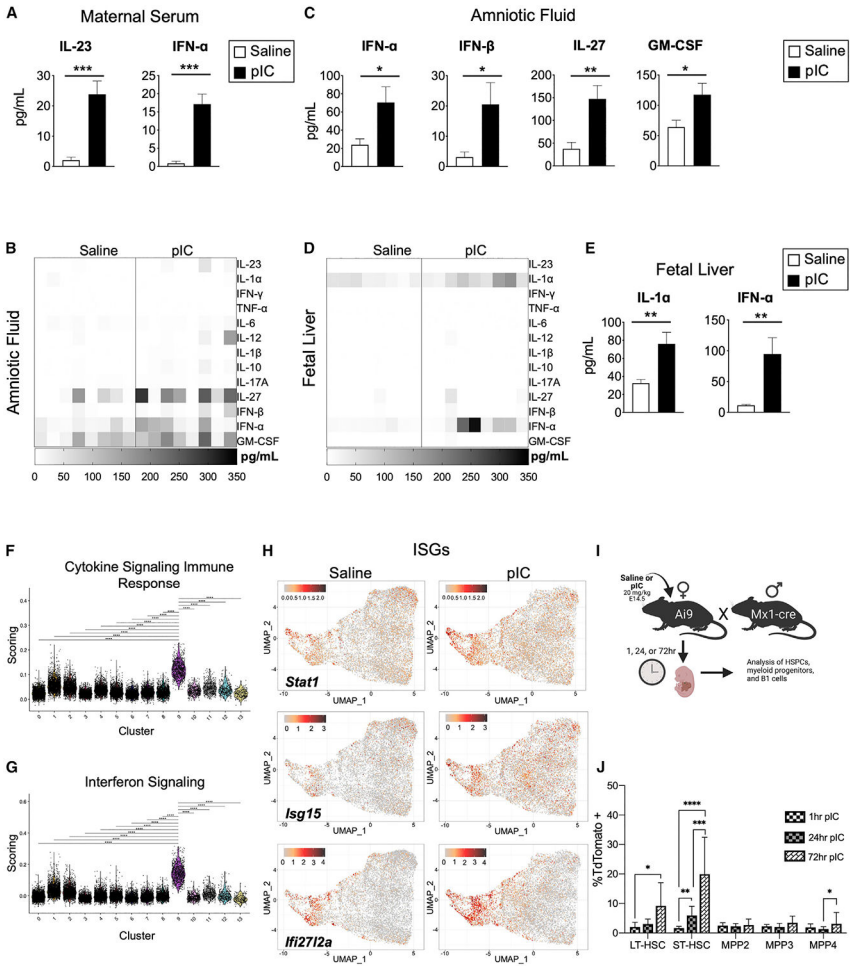

Figure 5. MIA-induced inflammatory cytokines specifically activate fetal HSPCs

(A) Absolute quantification of cytokines in maternal serum at E15.5 as measured by LEGENDplex assay. Data represent average ± SD. N = 3 per condition with three technical replicates.

(B) Heatmap displaying cytokines measured in amniotic fluid collected from E15.5 fetuses in litters following pIC or saline.

(C) Absolute quantification of significantly upregulated cytokines in AF at E15.5. Data represent average ± SD. N = 4 per condition with two technical replicates.

(D) Heatmap displaying cytokines in FL supernatant at E15.5 following pIC or saline.

(E) Absolute quantification of significantly upregulated cytokines in FL supernatant at E15.5. For all experiments, N = 3 litters/condition with three pups/litter. Data represent average ± SD.

(F) Single-cell RNA sequencing clusters scored against database of pathways (reactome.org) integral to cytokine signaling in the immune system. Scoring indicates enrichment assessed by the AddModuleScore function within individual clusters. Wilcoxon signed rank test.

(G) Single-cell RNA sequencing clusters scored against (reactome.org) database of pathways integral to IFN signaling in the immune system. Scoring indicates enrichment assessed by the AddModuleScore function within individual clusters. Wilcoxon signed rank test.

Author Manuscript Author Manuscript Author Manuscript Author Manuscript

(H) UMAP plots showing expression levels of genes associated with IFN alpha receptor (IFNAR) signaling following treatment with pIC or saline. Color bar indicates the relative expression level.

(I) Schematic of Mx1 Cre lineage-tracing experiments. Mx1-Cre males were crossed to Ai9 reporter females, and pregnant females were treated with 20 mg/kg pIC or saline at E14.5.

(J) Frequency of cells labeled by Tom+fluorescence in FL HSPC populations 1, 24, and 72 h following induction of Mx1-Cre by prenatal pIC or saline. Frequency of label (%TdTomato+) was determined by taking the average background labeling in saline-treated controls and subtracting it from the frequency of label in pIC-treated mice. N = 6–14 representative of at least two independent experiments. Data represent average ± SD.

Author Manuscript Author Manuscript Author Manuscript Author Manuscript

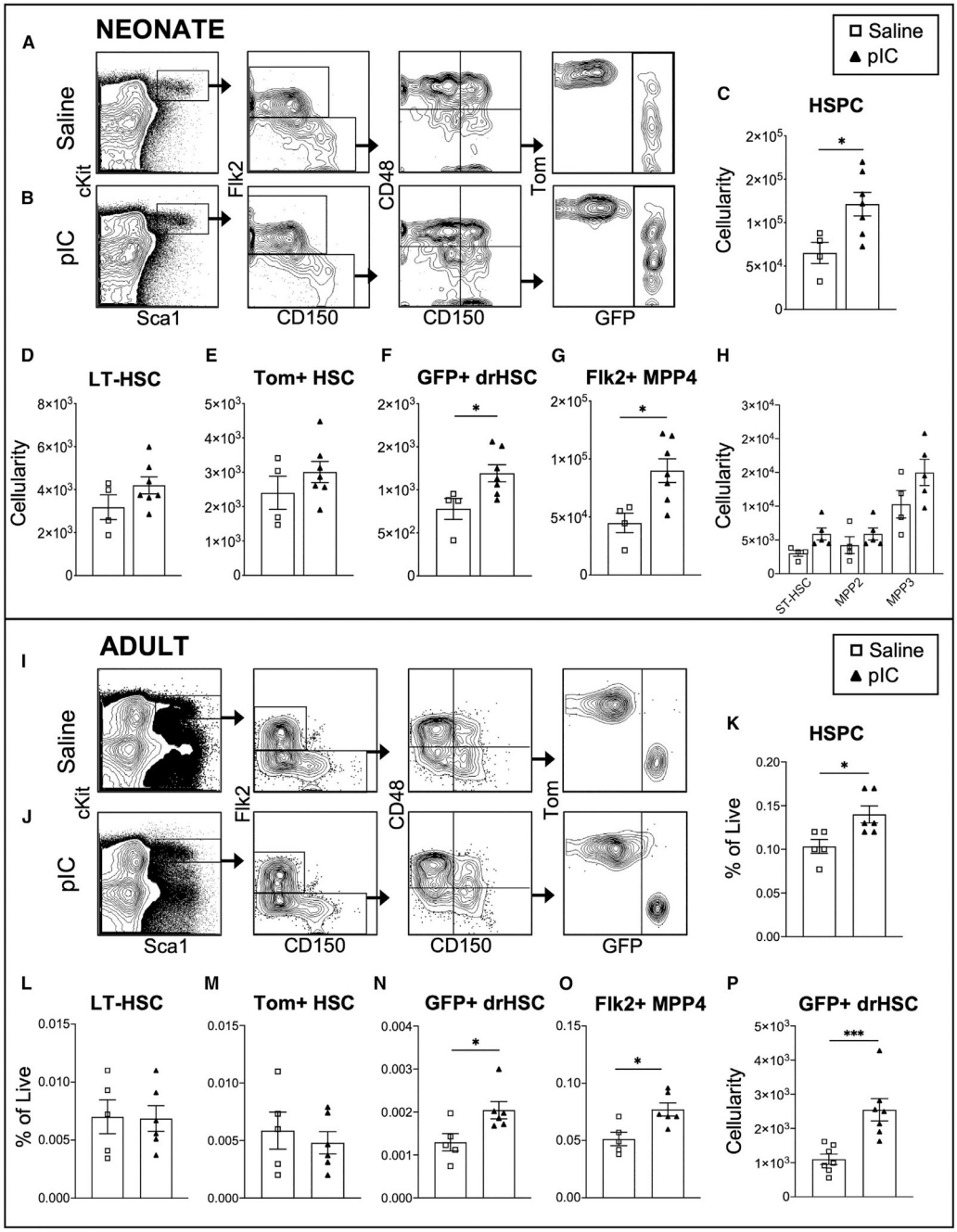

Figure 6. Prenatal inflammation induced by MIA affects postnatal hematopoiesis

(A and B) Representative FACS plots indicating gating of the BM HSPC compartment in saline (A) or pIC-treated (B) offspring at postnatal day (P)14. Tom+ HSC and GFP+ drHSCs are denoted by fluorescence within the LT-HSC compartment in FlkSwitch mice.

(C–H) Absolute quantification of HSPCs (gated as shown in Figure 2A) including total HSPCs (C), LT-HSCs (D), Tom+ HSCs (E), GFP+ drHSCs (F), Flk2+ MPP4s (G), and ST-HSCs, MPP2s, and MPP3s (H). N = 4–7 pups per litter, at least three litters per condition. Data represent average ± SEM.

Author Manuscript Author Manuscript Author Manuscript Author Manuscript

(I and J) Representative flow cytometric analysis of BM HSPC compartment at adulthood (8–10 weeks) from saline (I) or pIC-treated (J) litters.
(K–O) Frequency of adult BM HSPCs (gated as shown in Figure 2A) including total HSPCs (K), total LT-HSCs (L), Tom+ HSCs (M), GFP+ drHSCs (N), and Flk2+ MPP4 (O). Frequency of additional HSPCs can be found in Figure S5F. Data represent average ± SEM.
(P) Absolute quantification of GFP+ drHSCs. Absolute quantification of additional HSPCs can be found in Figures S5A-S5E. N = 6 representing at least three separate litters/ experiments per condition. Data represent average ± SEM.

Author Manuscript Author Manuscript Author Manuscript Author Manuscript

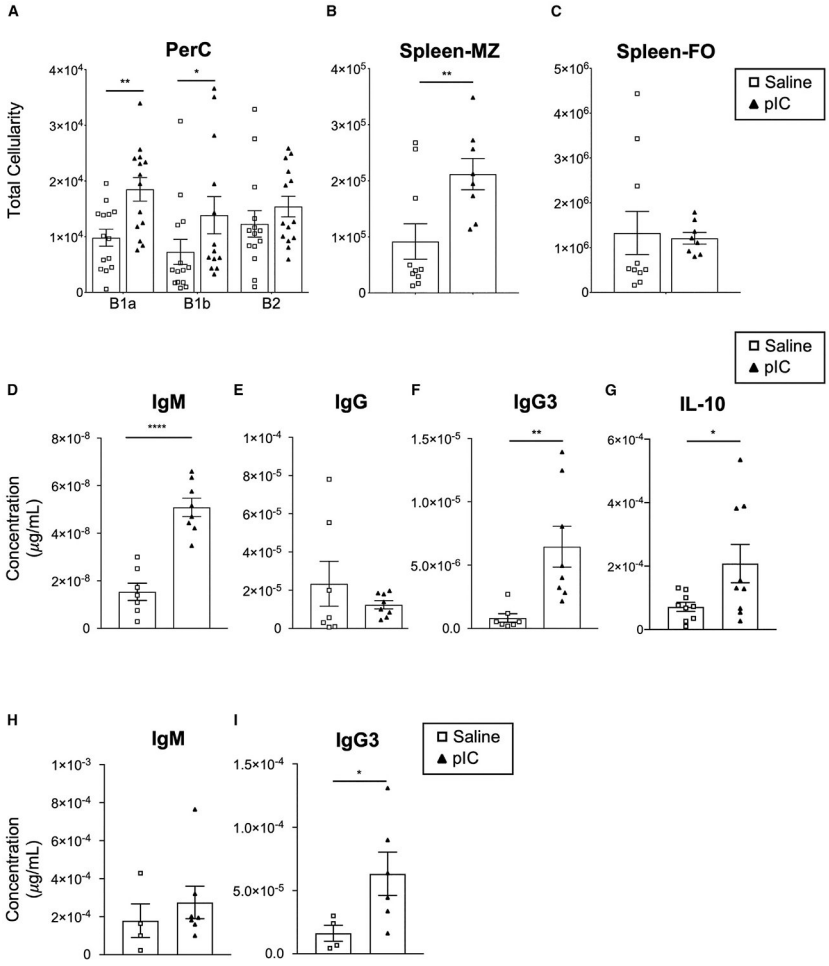

Figure 7. Prenatal inflammation induced by MIA shapes the function and output of fetal-derived immune cells

(A) Absolute quantification of peritoneal IgM+ B cell subsets, B1-a (CD5+CD11b+), B1-b (CD5−CD11b−) and B2 (CD5−CD11b−) cells in P14 offspring following pIC or saline at E14.5. N = 7–14 representing a least three litters per condition. Data represent average ± SEM.

(B and C) Absolute quantification of marginal zone (MZ; CD21+CD23−) (B) and follicular zone (FZ; CD21−CD23+) (C) IgM+ B cells in the spleens of P14 offspring following pIC or saline treatment at E14.5. N = 7–14 representing a least three litters per condition. Data represent average ± SEM.

(D–F) Quantification of peritoneal IgM (D), total IgG (E), and IgG3 (F) by ELISA normalized for cellularity in pIC- and saline-treated offspring at P14. N = 3 independent experiments representing three independent litters per group. Data represent average ± SEM.

(G) Quantification of IL-10 production following stimulation with Lipopolysaccharides (LPS) and Phorbol 12-myristate 13-acetate (PMA) of equivalent numbers of peritoneal B-1 cells isolated from P21 offspring following pIC or saline treatment at E14.5. N = 3 independent experiments representing three independent litters per group. Data represent average ± SEM.

Author Manuscript Author Manuscript Author Manuscript Author Manuscript

(H and I) Quantification of adult (8–12 weeks) peritoneal IgM (H) and IgG3 (I) normalized for PerC cellularity in pIC- or saline-treated offspring. Quantified using LEGENDplex Mouse Immunoglobulin Isotyping Panel. Data represent average ± SEM. N = 4–7 representing at least two separate litters/experiments per condition.

Author Manuscript Author Manuscript Author Manuscript Author Manuscript

KEY RESOURCES TABLE

REAGENT or RESOURCE	SOURCE	IDENTIFIER
Antibodies		
B220-BV605	Biolegend	RRID AB_2563312 (BioLegend Cat. No. 103244)
CD105-PE-Cy7	eBioscience	RRID AB_2573380 (Thermo Fisher Scientific Cat. No. 25-1051-82)
CD11b-Biotin	Biolegend	RRID AB_312787 (BioLegend Cat. No. 101204)
Cd11b-PB	Tonbo Biosciences	RRID AB_2621936 (Tonbo Biosciences Cat. No. 72-0112)
Cd11b-PE-Cy7	Tonbo Biosciences	RRID AB_2621836 (Tonbo Biosciences Cat. No. 60-0112)
CD150-BV785	Biolegend	RRID AB_2565962 (BioLegend Cat. No. 115937)
CD150-PE-Cy7	Biolegend	RRID AB_756199 (BioLegend Cat. No. 122514)
CD16/32	Biolegend	RRID AB_312801 (BioLegend Cat. No. 101302)
CD16/32-APC	Biolegend	RRID AB_1953273 (BioLegend Cat. No. 101326)
CD19-APC-Cy7	Biolegend	RRID AB_830707 (BioLegend Cat. No. 115530)
CD19-Biotin	Biolegend	RRID AB_313639 (BioLegend Cat. No. 115504)
CD1d-BV605	BD Biosciences	RRID AB_2740098 (BD Biosciences Cat. No. 740366)
CD21-PE-Cy7	eBioscience	RRID AB_1518766 (Thermo Fisher Scientific Cat. No. 25-0211-82)
CD23-e450	Biolegend	RRID AB_2571987 (BioLegend Cat. No. 101630)
CD3-APC	Biolegend	RRID AB_312677 (BioLegend Cat. No. 100312)
CD3-Biotin	Biolegend	RRID AB_312669 (BioLegend Cat. No. 100304)
CD4-Biotin	Biolegend	RRID AB_312689 (BioLegend Cat. No. 100404)
CD41-BV421	Biolegend	RRID AB_2650893 (BioLegend Cat. No. 133912)
CD45.2-BV605	Biolegend	RRID AB_2563485 (BioLegend Cat. No. 109841)
CD45.2-BV785	Biolegend	RRID AB_2562604 (BioLegend Cat. No. 109839)
CD48-APC	Biolegend	RRID AB_571997 (BioLegend Cat. No. 103412)
CD48-BV605	Biolegend	RRID AB_2650825 (BioLegend Cat. No. 103441)
CD5-AlexaFluor647	Biolegend	RRID AB_2075301 (BioLegend Cat. No. 100614)
CD5-Biotin	eBioscience	RRID AB_466340(Thermo Fisher Scientific Cat. No. 13-0051-85)
CD61-APC	Biolegend	RRID AB_2234024 (BioLegend Cat. No. 104314)
CD8α-Biotin	Biolegend	RRID AB_312743 (BioLegend Cat. No. 100704)
cKit-APC-Cy7	Biolegend	RRID AB_1626278 (BioLegend Cat. No. 105826)
cKit-BV605	Biolegend	RRID AB_2562042 (BioLegend Cat. No. 135122)
ESAM-PE-Cy7	Biolegend	RRID: AB_2860680 (Biolegend Cat. No. 136212)
ESAM-APC	Biolegend	RRID: AB_2101658 (Biolegend Cat. No. 136207)
F4/80-Biotin	Biolegend	RRID AB_893501 (BioLegend Cat. No. 123106)
Flk2-APC	Biolegend	RRID AB_2107050 (BioLegend Cat. No. 135310)
Gr-1-Biotin	Tonbo Biosciences	RRID AB_2621652 (Tonbo Biosciences Cat. No. 30-5931)
Gr-1violetFluor450	Tonbo Biosciences	RRID AB 2621968 (Tonbo Biosciences Cat. No. 75-5931)
IgD-BV785	BD Biosciences	RRID AB_2738322 (BD Biosciences Cat. No. 563618)
IgM-A647	Biolegend	RRID AB_2563479 (BioLegend Cat. No. 406526)
IgM-PE-Cy7	Biolegend	RRID AB_10642031 (BioLegend Cat. No. 406514)

Author Manuscript Author Manuscript Author Manuscript Author Manuscript

REAGENT or RESOURCE	SOURCE	IDENTIFIER
IL7Rα-PE-Cy7	Biolegend	RRID AB_2621859 (Tonbo Biosciences Cat. No. 60-1271)
Ki67-APC	eBioscience	RRID AB_2688057 (Thermo Fisher Scientific, Cat. No. 17-5698-82)
Nk1.1-Biotin	Biolegend	RRID AB_313391 (BioLegend Cat. No. 108704)
Sca1-APC-Cy7	Biolegend	RRID AB_756199 (BioLegend Cat. No. 122514)
Sca1-PB	Biolegend	RRID AB_2143237 (BioLegend Cat. No. 122520)
Sca1-PECy7	Biolegend	RRID AB_756199 (BioLegend Cat. No. 122514)
Ter-119-Biotin	Biolegend	RRID AB_313705 (BioLegend Cat. No. 116204)
Ter-119-PE-Cy5	eBioscience	RRID AB_468811 (Thermo Fisher Scientific Cat. No. 15-5921-83)
TLR3-APC	Biolegend	RRID AB_2561437 (Biolegend Cat. No. 141906)
IgM, unconjugated	Southern Biotech	RRID AB_2629437 (SouthernBiotech Cat. No. 101-10)
IgG, unconjugated	Southern Biotech	RRID AB_2732898 (SouthernBiotech Cat. No. 107-01)
Goat Anti-Mouse IgG1	Southern Biotech	RRID AB_2629437 (SouthernBiotech Cat. No. 1070-05)
Goat Anti-Mouse IgG3	Southern Biotech	RRID AB_2732898 (SouthernBiotech Cat. No. 107-01)
Chemicals, peptides, and recombinant proteins		
ACK Lysing Buffer	Thermo Fisher	Thermo Fisher Scientific Cat. No. A1049201
Calibrite Beads - APC	BD Biosciences	BD Biosciences Cat. No. 340487
CD117 Microbeads, Mouse	Miltenyi Biotech	Miltenyi Biotech Cat. No. 130-091-224
DMSO	Sigma	Sigma Cat. No D2650
FBS	Gibco	Thermo Fisher Scientific Cat. No. 26140079
Hoescht 33342	Invitrogen	Thermo Fisher Scientific Cat. No. H3570
LPS	Invivogen	Fisher Scientific Cat. No. NC0202558
PC-BSA	Biosearch Technologies	Biosearch Technologies Cat. No. PC-1011-10
PMA	Fisher Scientific	Fisher Scientific Cat. No. BP685-1
Propidium Iodide	VWR	WVR Cat. No. 89139-064
Polyinosinic:polycytidylic acid	Millipore Sigma	Millipore Sigma Cat. No. P1530
Streptavadin-PE-Cy5	Biolegend	Biolegend Cat. No. 405205
Tween 20	Fisher Scientific	Fisher Scientific Cat. No. BP337-100
StemPro-34 (1X)	Thermo Fisher	10639011
L-Glutamine	Thermo Fisher	25030149
Primocin	Fisher	NC9141851
SCF	Peprotech	250-03
Flt3L	Peprotech	250-31L
TPO	Peprotech	315-14
Critical commercial assays		
True Nuclear Transcription Factor Buffer Set	Biolegend	Biolegend Cat. No. 424401
LEGENDplex Custom Mouse 13plex panel	Biolegend	N/A
LEGENDplex Murine Immunoglobulin Isotyping Panel (6-plex) w/Vbp	Biolegend	740493
BD OptEIA Mouse IL-10 ELISA Set	BD Biosciences	BD Biosciences Cat. No. 555252
Rneasy Mini Kit	Qiagen	Qiagen Cat. No. 74106
Deposited data		

Author Manuscript Author Manuscript Author Manuscript Author Manuscript

REAGENT or RESOURCE	SOURCE	IDENTIFIER
scRNA-seq	This paper	GSE161927
Experimental models: Organisms/strains		
Mouse: C57BL/6J	The Jackson Laboratory	RRID:IMSR_JAX:006965
Mouse: mT/mG	The Jackson Laboratory	RRID:IMSR_JAX:007576
Mouse: *Flk2-Cre (Flt3-Cre)*	N/A	T. Boehm and C. Bleul (Max Planck, Freiburg, Germany)
Mouse: Ai9	The Jackson Laboratory	RRID: IMSR JAX:007909
Mouse: Mx1-Cre	The Jackson Laboratory	RRID: IMSR JAX:003556
Mouse: $TLR3^{KO/KO}$	The Jackson Laboratory	RRID:IMSR_JAX:005217
Oligonucleotides		
TLR3 Mutant Primer: GCC AGA GGC CAC TTG TGT AG	The Jackson Laboratory	oIMR7415
TLR3 Wild Type Forward Primer: GCA ACC CTT TCA AAA ACC AG	The Jackson Laboratory	oIMR7577
TLR3 Common Primer: AAT TCA TCA GTG CCA TGA GTT T	The Jackson Laboratory	oIMR7578
Software and algorithms		
Rstudio	RStudio	RRID SCR_000432
Flowjo v.10	Treestar	RRID SCR_000410
Graphpad Prism v.8	Graphpad	RRID SCR_015807
BD FacsDiva	BD Biosciences	RRID SCR_001456
snakePipes	Bhardwaj et al. (2019)	https://github.com/maxplanck-ie/snakepipes
STARsolo	Dobin et al. (2013)	https://github.com/alexdobin/STAR/blob/master/docs/STARsolo.md
Deeptools QC	Ramírez et al. (2016)	https://deeptools.readthedocs.io/en/develop/
Seurat	Satija et al. (2015)	RRID SCR_007322
DEseq2	Love et al. (2014)	RRID:SCR_015687